Wear 558–559 (2024) 205585

Contents lists available at ScienceDirect

Wear

journal homepage: www.elsevier.com/locate/wear

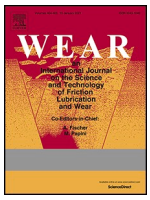

Wear properties of a new Al80Mg10Si5Cu5 multicomponent alloy

Ester Villanueva [a], Iban Vicario [a], Joseba Albizuri [b,*], Gurutze Arruebarrena [c], Teresa Guraya [b]

[a] Metal Processing Platform, TECNALIA, Basque Research and Technology Alliance (BRTA), Derio, Spain
[b] Faculty of Engineering of Bilbao (UPV/EHU), Department of Mechanical Engineering and Metallurgy, 48013, Bilbao, Spain
[c] Mechanical and Manufacturing Department, Mondragon University, Arrasate-Mondragon, Spain

ARTICLE INFO

Keywords:
Ball on disc
Friction
Wear
Aluminium multicomponent alloy
Abrasion

ABSTRACT

The present study investigates the tribological properties of a newly developed multicomponent aluminium weight-light multicomponent alloy for wear based on the Al80Mg10Si5Cu5 system for lightweight automotive applications, especially back drum discs. The samples were manufactured by High-Pressure Die Casting (HPDC) employing cast alloy returns and secondary aluminium ingots and were tested at room temperature (RT) and 200 °C. It has been observed that the Al80Mg10Si5Cu5 alloy offers a higher hardness and wear resistance at RT and especially at 200 °C compared with the AlSi9Cu3 reference alloy (x10 times reduction in wear rate). The impact of maintaining the external surface layer (skin) of HPDC cast parts has been studied for the ball-on disc test, showing improved tribological properties and the possibility of avoiding the machining of contact surfaces. The as-cast Al80Mg10Si5Cu alloy with the surface layer showed a wear rate coefficient of 5×10^{-4} $mm^3/N.m^2$ at RT, a 50 % lower than that of the sample without skin. Solution heat-treated samples (72 h at 440 °C, water quenching at 75 °C, and natural aging) with the surface layer showed a wear rate coefficient of 11×10^{-4} $mm^3/N.m^2$, approximately 20 % lower than the sample without a surface layer. The wear rate of AlSi9Cu3 alloy decreased by more than 50 % in the samples without skin at RT. At 200 °C, wear rate coefficients were lower in the samples with the surface layer.

1. Introduction

Aluminium multiphase and non-equiatomic High Entropy Alloys (HEA) alloys based on the multi-component concept have been demonstrated to own excellent physical and mechanical properties, in contrast to single-phase alloys [1]. The effect of rapid solidification processes to obtain enhanced single-phase microstructures in these alloys has been collected in recent works [2]. On the other hand, the demand for lightweight vehicles in the industry causes rapid growth in the manufacture of aluminium casting parts, especially for electric vehicles with the GIGAPRESS technology by High-Pressure Die Casting (HPDC) [3]. The electric vehicle market is continuously increasing, and lightning is critical to increase car autonomy. Aluminium drum brakes can be used for lighting electric cars, because the forces of rear brakes are lower than front brakes, and by using Kinetic Energy Recovery Systems (KERS), reducing brake forces. Also, front disk brakes act before rear drum brakes, with reduced pressure in the rear brakes [4]. Aluminium drums are lighter than iron drums, with improved heat dissipation and reduced fade, avoiding the possible corrosion of grey cast iron discs and disc failures [5].

AlSiCu are the most common aluminium alloys used in HPDC, but they present certain limitations in their mechanical properties [6] with AlSiMgCu alloys providing higher corrosion and higher strength, being generally improved by heat treatments, which makes them suitable for different automotive parts requiring good wear resistance and friction [7,8]. Insufficient wear resistance is a problem for aluminium alloys [9], though the tribological properties of Al alloys can be enhanced by balancing the type and quantity of alloying elements, or by introducing ex-situ reinforcing phases and by heat treatments [10–12]. To replace cast iron brakes and reduce vehicle weight, aluminium-based metal matrix composite (AMC) brake rotors have been developed. AMCs have higher heat conductivity, lower density, and higher specific strengths than aluminium alloys. AMCs present a ductile aluminium matrix reinforced with hard ceramic particles such as Al_2O_3, SiC, and SiO_2 to obtain customized properties [13].

However, the main disadvantages of AMCs are their production cost (especially machinability cost), the difficulty in the control of particle size and distribution, because wear characteristics greatly depend on reinforcement volume and size of the reinforced particles [14], the complex casting processes, and mainly the low or difficult recyclability

* Corresponding author. Faculty of Engineering of Bilbao (UPV/EHU), Department of Mechanical Engineering and Metallurgy, 48013, Bilbao, Spain.
E-mail address: joseba.albizuri@ehu.eus (J. Albizuri).

https://doi.org/10.1016/j.wear.2024.205585
Received 7 August 2024; Received in revised form 26 September 2024; Accepted 28 September 2024
Available online 30 September 2024
0043-1648/© 2024 The Author(s). Published by Elsevier B.V. This is an open access article under the CC BY-NC-ND license (http://creativecommons.org/licenses/by-nc-nd/4.0/).

of returns and scraps.

The most common method of enhancing the wear properties of cast aluminium alloys that are not AMCs is silicon alloying. Increasing the Si fraction, more Si hard crystals are produced, increasing the hardness of the alloy and its wear resistance. For tribological applications, the hypereutectic Al-Si alloys (with Si > 13 wt%) are typically employed, with a primary phase of silicon combined with aluminium in the eutectic phase. The silicon phases' type, morphology, size, and distribution are crucial to enhance the friction and wear resistance, by supporting an important portion of the load in the aluminium matrix regions deformed plastically [15–17]. In these alloys, Si in combination with Mg tends to precipitate as Mg_2Si. An increase in the amount of Mg promotes an improvement in wear performance [18]. Complex intermetallic phases are key in preventing junction growth and adhesion in wear mechanisms. Alloys with high intermetallic phases have lower wear rates [19]. An increase in copper in the alloy increases the mechanical properties, reduces the corrosion resistance, and could increase porosity [20,21]. In AlSi7Mg alloy, a minimum of 1 wt% Cu was needed to obtain the Al_2Cu intermetallic phase that promotes finer grains and increased hardness and wear resistance, lowering the friction coefficient [22]. The mechanism for improving the hardness of an aluminium cast alloy is also influenced by the reactions of Mg with Al and of Cu with Si, promoting different precipitates responsible of the strengthening of the alloy. The definition of the different phases' formation and their behaviour is a complicated task because several phases can precipitate near or at the same time, such as β (Mg_2Si), θ (Al_2Cu), S (Al_2CuMg) or Q ($Al_5Cu_2Mg_8Si_6$) [23]. During heat treatment, solution temperature, cooling rate, and time play an important role, resulting in several complex interactions. An aging process at an optimal temperature avoids the precipitation of large and non-coherent particles that could decrease strength and ductility. The combination of small amounts of other elements, as Fe, Mn, and Cr improves the hardness and strength of Al-Si alloys, increasing the wear resistance [24].

Focus on tribology studies of casting aluminium alloys, systems such as AlSi and AlSiCuMg(X) [25–27] are the most studied. In high silicon aluminium alloys, in general, the wear mechanism variates from ductile delamination, abrasive, and brittle delamination to ploughed abrasive wear by increasing the load [28]. Abrasion and oxidation are the dominant wear phenomena in the mild wear regime, but not always. Delamination, adhesion, and severe plastic deformation are the dominant in the severe wear regime in AlSi9Cu3 HPDC alloys [23]. Delamination has been related with the removal of large wear particles through the plastic deformation of the surface layer which occurs by subsurface crack nucleation followed by crack propagation [29,30]. This mechanism is particularly evident at elevated temperatures, where subsurface separation forms transfer layers that adhere and increase the coefficient of friction [31]. Additionally, it has been reported that the wear rate at high temperatures is ten times greater than at room temperature [32]. Under these conditions, a scuffing mechanism can occur, involving severe plastic deformation, material and layer transfer and accumulation. During high temperatures the adhesion between the layers can decrease, facilitating the delamination.

In some works, the wear mechanism changes with temperature from delamination to partial abrasive wear at RT to plastic deformation and oxidative wear (with plastic relaxation mechanisms becoming dominant) over 150 °C [33–36]. In the AlSi9Cu3 alloy, the hardness decreases, and also the mechanical and wear properties, because of the precipitation of different phases [23,24]. The wear rate is much higher at temperatures higher than 150 °C than at RT, but it does not have a linear proportionality with temperature, with a significant increase at about 200 °C. The increase of temperature of the wear test, in AMCs and aluminium alloys promotes higher compactness and higher average resistance of the surface layer, accelerating the oxidation of particles. If a surface layer is formed before the surface layer breakdown, the wear rate is reduced [6]. But if the surface layer is not compacted, the superficial particles are removed, the surface is damaged and delamination occurs, increasing the wear rate [23].

The mild to severe wear transition mechanism has been described by a combination of test variables such as the applied load, counter partner ball material, the sliding speed, and the contact surface temperature. Normally severe wear is related to a massive plastic deformation due to the thermal softening of the alloy and depending on the conditions, the aluminium alloys can work in a non-severe wear condition, controlling the delamination wear [9]. The conditions for obtaining a mild wear mechanism in AlSiCu(Fe) cast alloys have been studied [9,11,12,16, 37–39].

It is also noted that there is increased interest in using coatings for wear applications [40,41].

The ball on disc (BOD) test is one of the most employed tests for determining the wear properties of a material. The mechanism of wear rate analyzing the ball-on-disc test data can be divided into three main stages or phases [42–45]. The first phase corresponds to the removal of the surface layer with the maximum adhesion force between the base material and the ball because of the superficial asperities deformation and by increasing the number of residual particles. The second phase is normally related to the formation of a protective tribochemical surface layer or by a reduction in the ploughing and asperities deformation processes. There is sometimes a subphase when the rise in pin surface temperature can result in the formation of an oxide layer on the sliding surface, preventing the exposure of soft matrix material to the counter-ball surface, and reducing the wear rate of the pin surface [46, 47]. The third phase is characterized by an interfacial steady state of tribological conditions.

The applied load effect over the wear rate changes depending on the alloy, with some alloys showing weak wear rate at low loads, with a high increase in wear rate values at medium loads, and a gradual increase at high loads. Low applied pressure normally promotes the debris formed due to wear got trapped in the valley of the counter surface. Due to entrapment of debris in the valley, point contact by asperities from the disc is shifted to the contact surface. The shifting to contact surface and work hardening of samples led to steady-state wear [48,49].

An increase in applied pressure showed a temperature rise, leading to the removal of the oxide layer [48]. The fractured/fragmented oxide layer and the wear debris of counter surfaces can cause the formation of a mechanically mixed layer (MML) or transfer film (TF). Under the influence of applied pressure, the deformation of transfer film (TF) results in strain hardening of wear debris, increasing the hardness of the TF [48]. The constant formation and removal of the TF prevented the metal-to-metal contact, with the wear rate remaining constant in the steady-state-wear zone.

The transition from mild to severe wear values can vary from about 4 to 8 N up to 30 N [50] depending on the applied load. In general, the specific wear rate values increase with an increase in the applied load.

For commercial brake rotors, the Coefficient Of Friction (COF) has values between 0.45 and 0.69. For some authors, there is not a linear increase in COF value increasing the load [51] and for others, there is a linear increase for Al-Al_2O_3 MMC and Al-SiC MMC alloys for example with stable friction coefficients between 0.30 and 0.60 for brake rotor applications [52].

The reported wear rate for drum brakes to define a mild or severe wear state varies. Severe wear rates have been reported, with $k = 15 \times 10^{-3}$ mm^3/N.m for the Al7.1Si alloy [53], 6×10^{-3} mm^3/N.m for LM17 alloy, and $7.5–10 \times 10^{-3}$ mm^3/N.m for aluminium composites with pressure and velocity (0.2–1.0 N/mm^{-2} and 1.6 m/s respectively) representatives of braking conditions for brake rotors [54]. A LM27 alloy reinforced with rutile and sillimanite minerals Hybrid AMCs (HAMCs) for brake rotor applications showed wear rates at 500 m around 16.5×10^{-3} mm^3/N.m for a commercial rotor material and 18×10^{-3} mm^3/N.m for the HAMC, with final steady wear values around 6 and 7×10^{-3} mm^3/N.m respectively. Values between 0.37x10-^{4} to 2.37x10-^{4} mm^3/N.m are generally within the severe wear regime [55]. However, in the case of aluminium cast alloys, with a 15 N test force, they are around 5

$\times 10^{-3}$ mm^3/N.m [56]. To determine the charge of the test, 15 N has been selected to compare the results with the bibliographic information for aluminium brakes because of the high bibliographic data variation depending on the tested alloy [56].

The selection of ball material is crucial because it can modify final results. With aluminium alloys, alumina is often employed as the ball material to avoid the formation of the MML containing Al–Fe–O during the tests when steel balls are employed, due to the affinity of aluminium with steel [55–57], minimizing the chemically driven aspects of adhesive wear due to the minimal chemical-driven adhesion. So, the determination of the effect of the aluminium alloy on wear properties is easier with alumina counter ball [58].

The new developed Al80Mg10Si5Cu5 alloy has been designed to maintain its properties up to around 200 °C and the selection of alloying elements was carefully determined to obtain Mg_2Si and Al_2Cu intermetallic phases (that increase the wear resistance) but without the presence of primary Si (to obtain better mechanical properties and some ductility). The application of the newly developed alloy could be for aluminium drum brakes, especially for the rear brakes of small electric cars.

Recently, scrap-tolerant $Al_{65}Cu_{10}Mg_{10}Si_{10}Zn_5$ and $Al_{80}Cu_5Mg_5Si_5Zn_5$ HEA aluminium alloys have been studied, showing promising mechanical and wear properties [59] but there is still very little information on the wear properties of HEA aluminium alloys and less with materials produced by an industrial process based on secondary aluminium alloys or scraps. Secondary aluminium ingots, cast aluminium returns, and magnesium scraps melted in an electric crucible furnace and the HPDC processes were employed to obtain low CO_2 manufacturing values [60].

So, in this study, the developed alloy will be studied at RT and 200 °C and compared with the most standard casting alloy (AlSi9Cu3 alloy) in the as-cast and thermally treated (TT) state.

In parallel, aluminium casting parts produced by HPDC show a skin region (or surface layer) in the external surface, which is nearly free of defects with improved mechanical properties [61]. However, the effect of maintaining the external surface layer on the wearing properties in the ball-on-disk (BOD) test has not been or very scarce studied [62].

2. Materials and methods

2.1. Manufacturing

The experimental Al80Mg10Si5Cu5 and AlSi9Cu3 alloys were manufactured by HPDC, with a 950t injection machine (PT-650, Pretansa). For melting and holding the alloys, an electrical furnace of 500 kg capacity (Dugo EBC, Dugopa) was employed. As charge material, secondary aluminium alloy ingots of AlSi7Mg and AlSi9Cu3 were employed as melting bath and were alloyed with AM60B casting returns. When the target composition of the specific alloy was obtained, the working temperature was adjusted to 700 °C, and the molten metal was injected into the metal die with an alloy temperature of 680 °C and a die temperature of about 250 °C. Once solidified, casting parts were extracted and instantly immersed in water at the temperature of 50 °C. Plane plates for wear tests with a crosshead distance of 290 mm were obtained.

Some casting samples were subjected to a specified developed thermal treatment to improve the mechanical properties. The thermal treatment involved a solution treatment at 440 °C for 72 h, followed by water quenching at 75 °C, and natural ageing. The value of 75 °C for water quenching temperature after solution treatment was selected to reduce internal stresses. For the solution treatment, a chamber furnace with radiation heating was employed (LH 60/13, Naberthem).

2.2. Analysis of chemical composition

The composition of the experimental alloys was controlled during the casting process, by discharge optical emission spectrometry (OES, Spectro, Spectrolab).

2.3. Microstructural analysis

The microstructure of the two experimental alloys was characterized by an optical microscope (MO, DMI5000 M, Leica Microsystems), and the phases identified with a scanning electron microscopy SEM (FEI Quanta 200 ESEM), equipped with an energy dispersive X-ray spectrometry (EDS). Analysis software X-ray microanalysis (Pathfinder, ThermoFisher) was employed to obtain the images and data.

For the observation procedure, specimens were extracted from cast bars and prepared to employ standard metallographic procedures (hot mounting in conductive resin, grinding, and polishing).

2.4. X-ray powder diffraction tests

XRD patterns were obtained by employing a Philips X'Pert Pro MPD PW3040/60 X-ray diffractometer equipped with a copper anode operating with a 40 kV and 40 mA (1.6 kW) voltage. The scans were performed using Cu-Kα radiation equipment with a wavelength of 0,154184 nm in a 2θ range from 10° to 90°, with a step size of 0.02° 2θ and each stage lasting 2s. The X-ray diffraction patterns were indexed with the PDF-2 database from the International Center for Diffraction Data (ICDD).

2.5. Characterization of hardness properties

Hardness was measured using the Vickers diamond indentation test (FV-700, Vickers Indenter, Leica) with a load of 3 kg for 10 s according to UNE EN ISO 6507-1. At least ten readings were measured. Hardness was also measured at 200 °C, with samples heated in an electric furnace (3119-406 LCF, Instrom) for 30 min. After the established time, samples were extracted, and indentations were performed.

2.6. Wearing test

Dry sliding wearing friction tests were carried out over the new Al80Mg10Si5Cu5 alloy (as-cast and heat-treated conditions) and AlSi9Cu3 (as-cast condition) in a sphere-on-plate reciprocating configuration using a ball-on-disk mode tribometer (MT2/60/NI/HT, Microtest S.A.). Tests were performed at RT according to the ASTM G99-05 standard without any lubricant, and at 200 °C using a similar tribometer inside an insulated chamber. An electrically heated furnace on the bottom of the sample controlled by a K-type thermocouple was employed. Before the test, samples were heated to 200 °C at 0.1 °C/s Fig. 1 displays the equipment and procedure used for tribo-tests at RT and 200 °C.

6 mm diameter alumina balls were used for each test as counter-face bodies. An alumina ball pin was employed as a counter-partner to minimize the chemically driven aspects of adhesive wear. These alumina

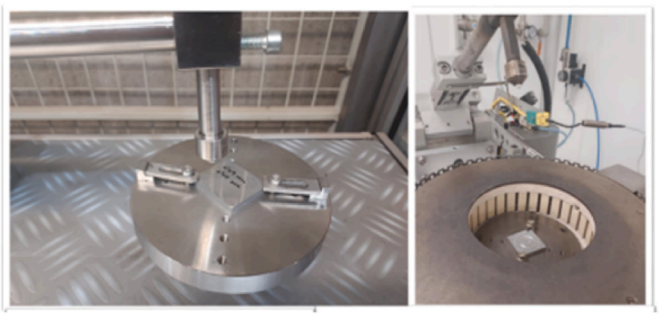

Fig. 1. Detail of tribometer employment and their components.

spheres have a hardness of 1250–1700 HV. Test conditions are summarized in Table 1. These parameters were selected to compare the wear rate of the Al80Mg10Si5Cu5 with the bibliographic values of AlSi9Cu3 alloy and other aluminium alloys at around 200 °C [63], selecting 15 N for the load so that it can be evaluated in aluminium drum brakes. The data acquisition and control of the coefficient of friction (COF) during the test was conducted through the MT4002 V12.0 (MT4002, Microtest S.A.) software connected to the tribometer. At least three times in each sample with a new alumina sphere in each test under identical conditions were performed to assure the repeatability of the measurement.

Specimens from plate-shaped casting parts were extracted and machined, obtaining test coupons of about 50 x 50 × 5 mm. Then samples were polished using diamond particles of 3 μm to guarantee a roughness value below the maximum recommended value [64]. Also, samples with the external surface layer were tested to investigate the effect of maintaining the casting surface layer, considering that the roughness could affect the wear and lubrication behaviour, the friction coefficient, and the load transmission [42]. The roughness of all samples was measured using a portable device (Rugosurf, TESA), with at least 10 measurements per sample. The resulting mean roughness (Ra) of samples with the surface polished was Ra <0.1 μm and Ra <1.0 μm for samples with the surface layer.

The testing parameter for revolutions per minute was slightly higher at 123.33 rpm, and the rest of the variables were as follows [23].

After each experiment, the wear rate was determined by 3D laser scanning confocal microscopy (DCM 3D, Leica). This technique allows for measuring the real shape of the wear track [65]. A total area of 20.8 × 20.2 mm and 684 μm height was measured using a 5× objective. Fig. 2 shows a sample of a surface topography image of the wear track from which the total wear area was determined, measuring at least 16 2D profiles with the Leica map software. Then, the total loss volume was calculated, and wear coefficients were obtained in mm^3/N.m [66,67]. Finally, the wear surface and subsurface were analyzed to determine the wear mechanisms, using a SEM scanning electron microscope equipped with EDS.

The specific wear rate w (mm^3/N.m) was calculated using the following **Equation (1)**:

$$w = V/s \times F \qquad \text{Equation 1}$$

where V represents the volume loss (mm^3), s (m) is the total sliding distance and F(N) is the applied load.

3. Results and discussion

3.1. Chemical composition of the experimental alloys

We can observe in Table 2, the obtained chemical composition in weight percentage of each alloying element for Al80Mg10Si5Cu5 and AlSi9Cu3 alloys. The alloy Al80Mg10Si5Cu5 was composed principally of aluminium (around 80 % wt.), magnesium (10 % wt.), and silicon and copper of almost equal weight (5 % wt.). AlSi9Cu3 alloy presented a chemical composition in agreement with the EN 1706:2020 standard.

We can observe in Table 2, also the presence of Fe and Mn in the Al80Mg10Si5Cu5 alloy. A percentage of about 0.25 wt% of Fe and approximately a half of the total content of Fe of Mn (0.13 wt%) has been carefully obtained from the combination of the different raw materials to avoid the presence of the well-known β-Al5FeSi detrimental phase and to avoid metal soldering in the die. In the case of the AlSi9Cu3 alloy, the sludge factor (SF) of the alloy, calculated by Refs. [68,69] is 1.0:

$$SF = (wt.\%Fe \times 1) + (wt.\%Mn \times 2) + (wt.\%Cr \times 3) \qquad \text{Equation 2}$$

Table 1
Wearing test parameters.

Test Parameters	Selected Value(s)
Load (N)	15.0
Velocity (m/s)	0.1
Rotation speed (rpm)	127.3
Sliding distance (m)	500.0
Track diameter (mm)	15
Environment	Dry air

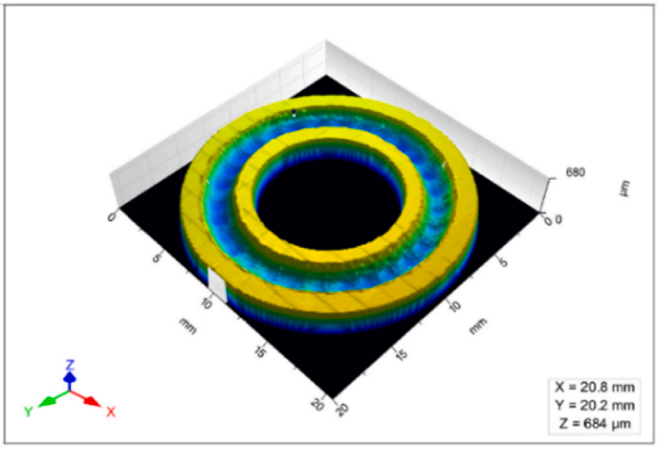

Fig. 2. Detail of wearing surface topography.

Table 2
Obtained chemical composition for studied alloys in %wt.

Reference	Al	Si	Fe	Cu	Mn	Mg	Zn
Al80Mg10Si5Cu5	78.9	5.6	0.3	4.7	0.1	10.3	0.1
AlSi9Cu3	87.2	8.3	0.6	2.4	0.2	0.2	0.7

3.2. Phase composition

The determination of the different phases has been determined by XRD, and the results can be observed in Figs. 3 and 4. The new Al80Mg10Si5Cu5 alloy in the as-cast condition presented an aluminium matrix and phases of Mg_2Si, Al_2CuMg, and Al_2Cu. In the case of heat-treated Al80Mg10Si5Cu5 alloy, the Al_2Cu phase was not visible in the XRD analysis, and an Al matrix with Mg_2Si and Al_2CuMg phases was identified.

Al_2CuMg phases are more stable than Al_2Cu, and Al_2Cu tents to be transformed into Al_2CuMg by natural or artificial ageing on Al-Si alloys

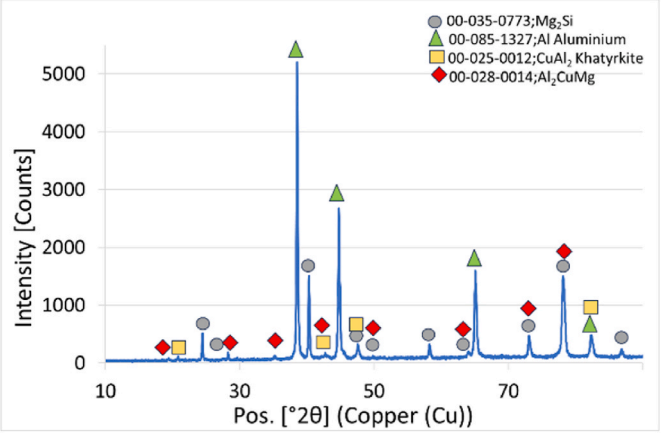

Fig. 3. XRD analysis of as-cast Al80Mg10Si5Cu5 alloy.

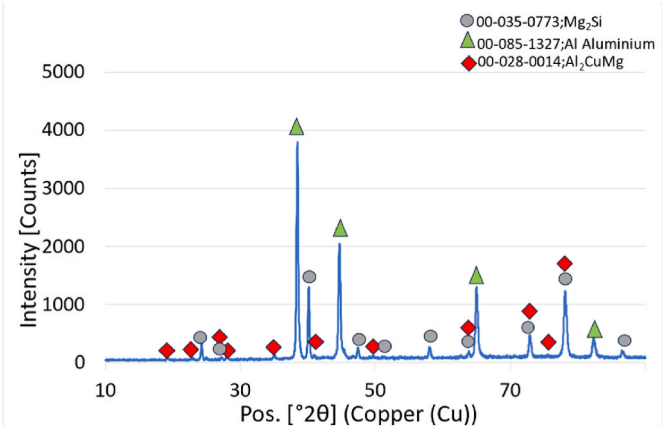

Fig. 4. XRD analysis of heat-treated Al80Mg10Si5Cu5 alloy.

containing Cu and Mg, in concordance with obtained results [70].

3.3. Microstructure analysis

A microstructural analysis has been performed to determine the microstructure and presented phases. Fig. 5 shows a detailed backscattered SEM microstructure of the as-cast Al80Mg10Si5Cu5 alloy.

In Table 3 we can observe the SEM + EDS composition of the different analyzed regions.

From the SEM + EDS analysis, we can observe that there are dark-grey aluminium dendrites enriched with the rest of the alloying elements (region A). Blocky black phases (region B) are distinguished. The big blocky phases are correlated with pre-dendritic Mg_2Si particles and the small ones with post-dendritic eutectic Mg_2Si particles. Light grey particles (region C) are formed into the interdendritic spaces, and they have been correlated with Al_2Cu phases. Finally, white phases (region D) are also precipitated into the interdendritic space, close to the light grey phases, and have been correlated with the Al_2CuMg phases. Some oxygen is also detected, mainly in the phases with the higher Mg content. That can be related to the fact that the melting process has been performed without any protective atmosphere, and Mg is very prompt to oxidize.

Fig. 6 shows the microstructure of the as-cast Al80Mg10Si5Cu5 alloy with the cast surface layer and Fig. 7 without the surface. They showed principally a matrix of aluminium, dark regions corresponding to phases of primary and eutectic Mg_2Si, and white precipitates presented at the

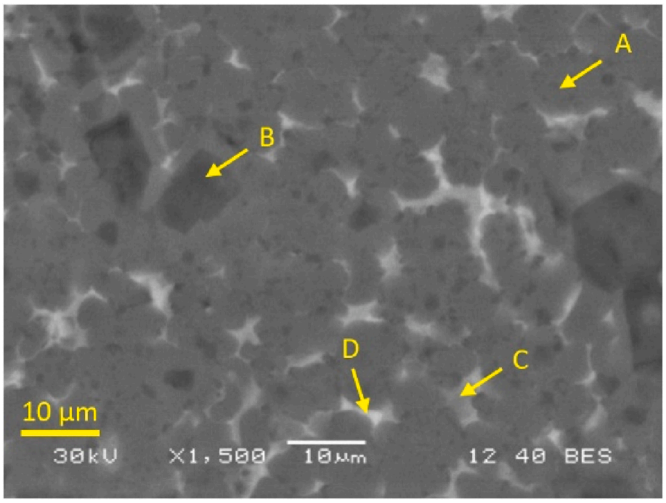

Fig. 5. Analyzed phases in as-cast Al80Mg10Si5Cu5 alloy.

Table 3
SEM + EDS composition of the identified regions in Al80Mg10Si5Cu5 alloy (wt. %).

Region	Al	Mg	Si	Cu	Fe	Mn	O
A	87.4	5.8	1.8	2.4	–	0.2	2.4
B	62.9	16.1	13.1	2.5	–	–	5.4
C	64.7	8.2	1.2	23.6	0.2	–	2.3
D	73.6	10.0	2.1	11.5	–	–	2.8

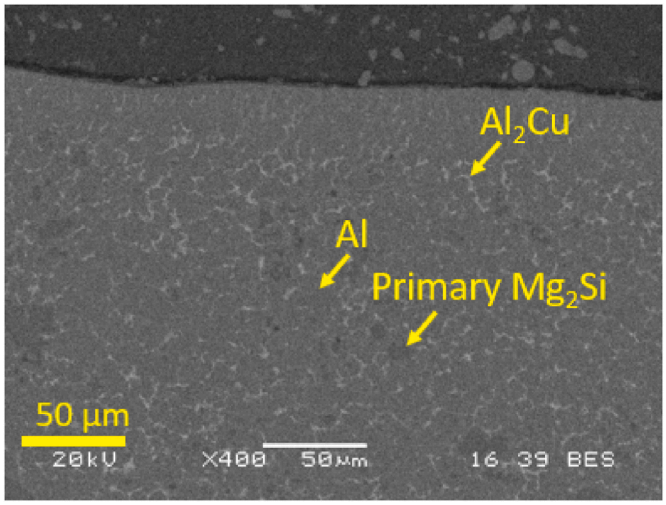

Fig. 6. Surface cast layer backscattered SEM images (x400 augmentation) of as-cast Al80Mg10Si5Cu5 alloy.

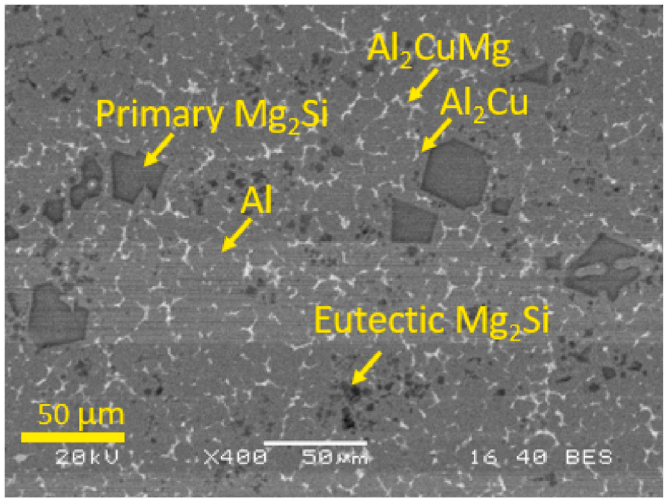

Fig. 7. Prepared sample backscattered SEM images (x400 augmentation) of as-cast Al80Mg10Si5Cu5 alloy.

interdendritic regions associated with Al_2Cu and Al_2CuMg phases.

The surface layer displayed a finer structure, with a smaller amount of eutectic Mg_2Si. The size of the intermetallic Al_2Cu and primary phases of Mg_2Si presented the smallest size in the surface layer. This is in line with other studies [61], where the external surface layer is formed by smaller grain size, contains fewer phases, and is nearly defect-free [71].

Fig. 8 shows the microstructure of the heat-treated Al80Mg10Si5Cu5 alloy with the surface layer and Fig. 9 without the surface layer. The Al80Mg10Si5Cu5 alloy in the TT state presented a globe-like shape microstructure resulting in an aluminium matrix, Mg_2Si, and Al_2CuMg phases. The Al_2Cu phase was not identified. The aspect and size of the

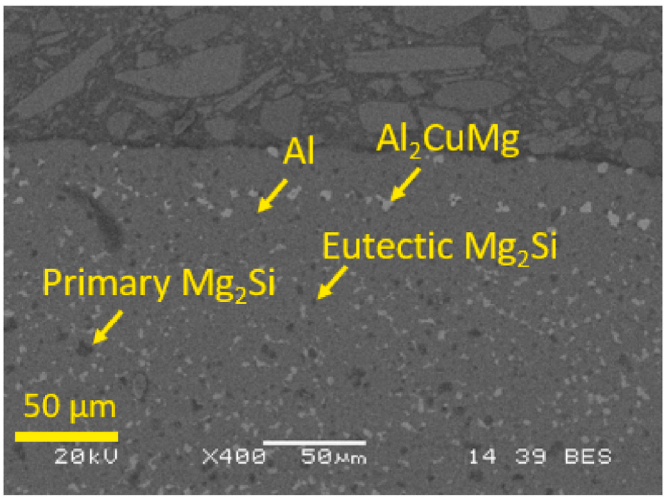

Fig. 8. Surface cast layer sample SEM images (x400 augmentation) of the heat-treated Al80Mg10Si5Cu5 alloy.

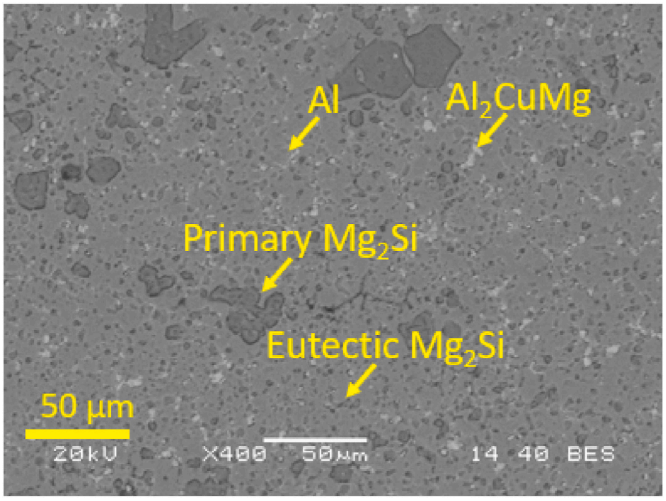

Fig. 9. Inner region sample SEM images (x400 augmentation) of the heat-treated Al80Mg10Si5Cu5 alloy.

phases presented quasi-similar microstructure in both regions of the sample.

Figs. 10 and 11 show the microstructure of as-cast AlSi9Cu3 alloy with the surface layer and without the surface layer. The AlSi9Cu3 alloy in the as-cast state presented a dendritic microstructure composed of an aluminium matrix, eutectic silicon (Al + Si), and Al_2Cu intermetallic phases in the eutectic region. The sample with the surface layer showed a finer dendritic microstructure. On the contrary, segregated sludge particles were distinguished in the inner region, with more interdendritic porosity [23].

3.4. Hardness properties

The measured hardness values of the experimental alloys in the surface layer (S) and the inner region (I) are presented in Table 4 at RT and 200 °C.

The hardness of the samples was slightly higher in the surface layer, due to finer grain size and the smaller presence of microporosity. We can observe also how the as-cast Al80Mg10Si5Cu5 alloy has a higher hardness than the TT-Al80Mg10Si5Cu5 alloy, and the lowest hardness value is obtained with the AlSi9Cu3 alloy. So, as in the case of cast aluminium alloys, a higher hardness is expected to lead to higher wearing resistance results [24].

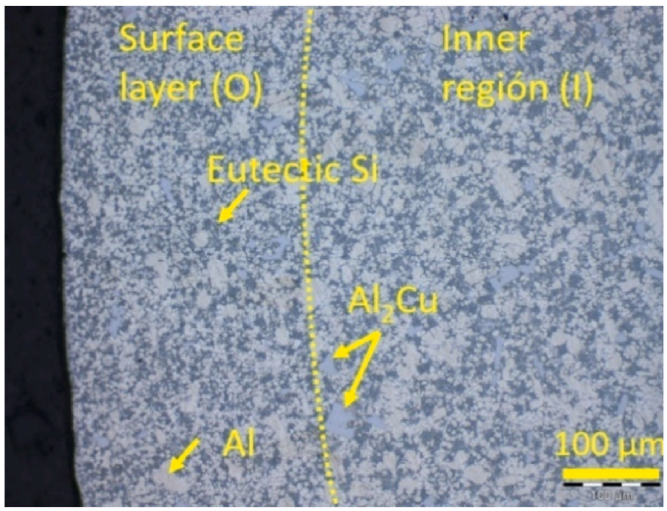

Fig. 10. Outside region optical microscopy images (x200 augmentation) of as-cast AlSi9Cu3 alloy.

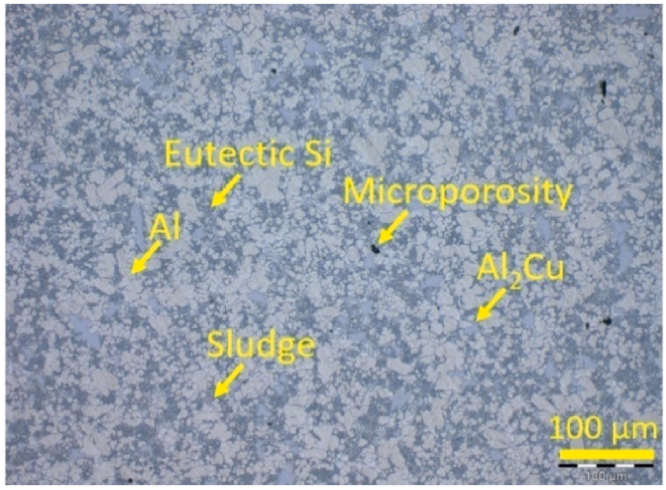

Fig. 11. Inner region optical microscopy images (x200 augmentation) of as-cast AlSi9Cu3 alloy.

Table 4
HV3 Values of studied alloys at different temperatures.

Reference	Hardness (HV3)			
	RT		200 °C	
	S	I	S	I
Al80Mg10Si5Cu5 as-cast	136 ± 5	130 ± 13	126 ± 4	121 ± 10
Al80Mg10Si5Cu5 TT	125 ± 6	114 ± 12	115 ± 4	106 ± 11
AlSi9Cu3 as-cast	114 ± 5	95 ± 7	103 ± 6	86 ± 8

3.5. Friction curve analysis at RT

Figs. 12 and 13 show the evolution of the coefficient of friction (COF) measured on as-cast and TT-Al80Mg10Si5Cu5 and AlSi9Cu3 alloy at RT with and without skin, line in blue (as-cast Al80Mg10Si5Cu5), green (TT-Al80Mg10Si5Cu5), and red (AlSi9Cu3).

Al80Mg10Si5Cu5 and AlSi9Cu3 alloys presented similar values for COF at RT. In the samples with skin, the obtained values are very similar for both alloys in the as-cast stage, but COF values increased slightly in

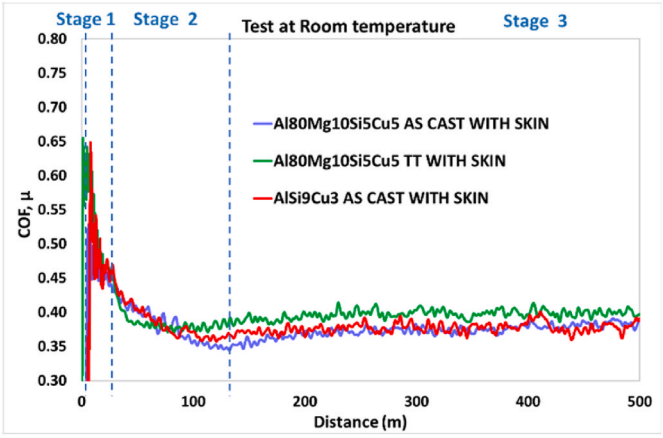

Fig. 12. Evolution of the coefficient of friction for the studied alloys at RT (0.1 m/s) with the surface layer.

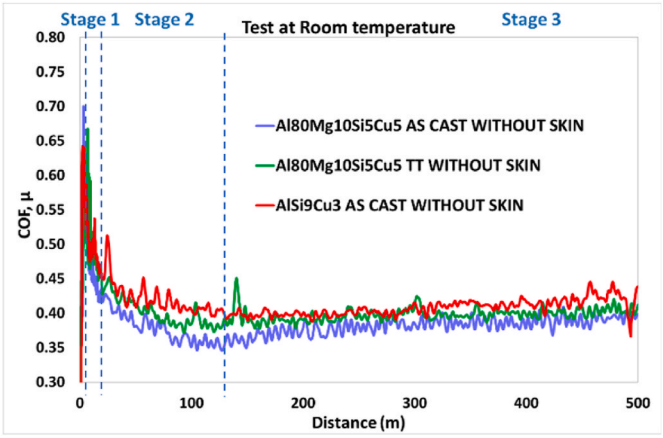

Fig. 13. Evolution of the coefficient of friction for the studied alloys at RT (0.1 m/s) without the surface layer.

the case of TT-Al80Mg10Si5Cu5 samples. It can be related to the observed modification of the microstructure in TT samples, with a more homogeneous microstructure and a reduction in the hardness. In this case, there is no direct correlation between the superficial hardness and COF values, probably because the smaller precipitates in the case of AlSi9Cu3 samples, including Fe-rich precipitates, that have high punctual hardness. In the samples without the external surface, there is a correlation between the obtained hardness and the COF values, corresponding the higher COF values to the lower hardness values, with AlSi9Cu3 with the highest COF values as expected. The samples without the surface layer presented COF higher values in all the cases. The absence of defects and smaller grain size and minor amount of eutectic in the external surface [61], contribute to increase the hardness [72].

The analyzed curves presented the 3-stage curve characteristic of metals, as reported in the literature [7,23,24]. In the different COF curves, the approximative stage positions are marked.

First, low values around 0.1 were measured (previous or zero phase), related to the settling of the materials in the test bar. In the case of the Al80Mg10Si5Cu5 and AlSi9Cu3 samples with the surface layer, the friction curve presented low COF values during the initial period, presenting a previous stage, because of the surface layer acting as a lubricant and superficial irregularities, [40]. A higher rugosity in the samples with the external surface promotes a reduction of the COF values in the previous or zero phase [73]. An initial rise in the coefficient of friction was correlated with abrasive and adhesive wear, concretely from galling. COF values increased with the distance run, reaching a maximum value of 0.60–0.70 (Stage 1). COF values increase when large-sized debris is accumulated on the worn surface, and they decrease when the debris is eliminated from the worn surface. In the sliding test, after approximately 100–150 m, the COF values gradually decreased to around 0.35–0.38. This stage corresponds to the transition period, occurring shortly after reaching the maximum peak and before the equilibrium phase.

Shearing of the junctions took place, and the coefficient felt off as the strong junctions, which were formed during quasi-static loading initial pressure, became replaced by weaker ones. After the plastic process starts, the surface is deformed enough to reduce the friction coefficient to the steady state value. The steady state is reached when the sliding force is higher than the friction force (Stage 3). All the obtained values are resumed in Table 5 to compare the results at the RT and 200 °C.

3.6. Analysis of friction curve at 200 °C

Figs. 14 and 15 show the evolution of the COF values measured for the samples of the Al80Mg10Si5Cu5 and AlSi9Cu3 alloys at 200 °C with and without skin of one representative sample. The evolution of COF values and the acting mechanisms were very different from tests at RT, between the as-cast state and the TT samples, and the alloys. In all the samples, there is a correlation between the obtained hardness and the COF values, corresponding to the higher COF values with the lower hardness values for AlSi9Cu3 alloy. However, the values for as-cast and TT samples were dissimilar, probably because the heating of the samples for preparing and performing the test promoted a partial aging of the microstructure of as-cast samples.

As-cast Al80Mg10Si5Cu5 alloy with and without the surface layer started with low COF values, around 0.1 (previous or zero phase). Then, increasing the distance, the COF value increased, reaching the maximum value of 0.45 (Stage 1). COF value decreased progressively (Stage 2). Finally, just after the highest peak, a steady value of around 0.43 was obtained (Stage 3), with slightly higher values than at RT, but without an expected high increase in the COF value. In aluminium alloys, as in AlSi9Cu3 alloy, temperatures higher than 150 °C decrease the hardness, mechanical, and wear properties [23]. In the samples with the surface layer, the maximum coefficient of friction is slightly smaller, possibly since at higher temperatures there is a higher oxidation of the surface layer and therefore smaller adhesion.

In the case of Al80Mg10Si5Cu5 alloy in TT conditions, COF value increased from the lower value (0.1) up to the value of 0.50–0.60, and finally reached the steady stage, with larger oscillations with a mean value of 0.47. These oscillations are possibly due to the entrapment and release of the debris particles between the sliding surfaces. This is consistent with some previous works [74–77] where higher abrasive particle sizes promote that the friction coefficient decreases. However, for fine abrasive particles, the tendency is reversed, being the adhesive-wear the main acting mechanism, and responsible for the increased COF values. It is noted that in the case of TT-Al80Mg10Si5Cu5 without the surface layer, the COF values during the distance run were higher.

AlSi9Cu3 alloy in the as-cast state showed that the COF values

Table 5
Values for COF at RT and 200 °C.

REFERENCE	Coefficient of friction μ (COF)			
	RT		200 °C	
	S	I	S	I
Al80Mg10Si5Cu5 as-cast	0.38 ± 0.006	0.38 ± 0.008	0.41 ± 0.022	0.42 ± 0.010
Al80Mg10Si5Cu5 TT	0.38 ± 0.008	0.39 ± 0.007	0.53 ± 0.051	0.50 ± 0.017
AlSi9Cu3 as-cast	0.37 ± 0.003	0.39 ± 0.019	0.64 ± 0.069	0.80 ± 0.110

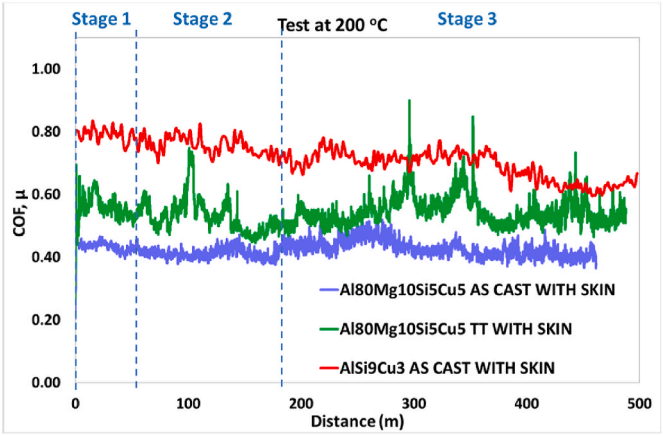

Fig. 14. Evolution of coefficient of friction for the experimental alloys at 200 °C (0,1 m/s) with the surface layer.

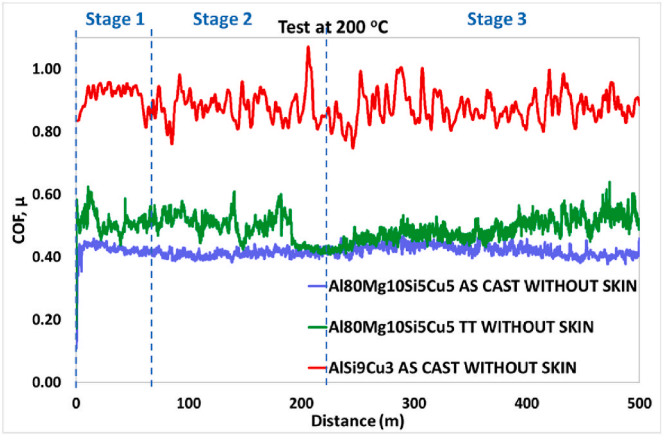

Fig. 15. Evolution of coefficient of friction for the experimental alloys at 200 °C (0,1 m/s) without the surface layer.

increased from a lower level up to 0.80, being the alloy with the highest COF values. It showed more fluctuations in its values. Big fluctuations have been previously correlated with a larger volume of intermetallics in the alloy, with an inverse relation between COF values and hardness values [78]. It could be also related to the presence of very hard Fe-rich intermetallics [24]. The lowest fluctuations and COF values are obtained in the Al80Mg10Si5Cu5 alloys.

Remarkably, the COF curve at 200 °C presented a three-stage behaviour in all the alloys, with the previous stage suppressed. The cause could be the effect of the temperature over the samples because a more intense mechanism of plastic deformation and delamination takes place. It was demonstrated that the AlSi9Cu3 alloy showed higher average dynamic friction values than the Al80Mg10Si5Cu5 alloy, with a downward trend that is characteristic when the abrasion mechanism predominates [45] in Al80Mg10Si5Cu5 alloy.

In Table 5, mean values for the coefficient of friction at the different temperatures are collected.

As it has been described, the experimental alloys showed similar behaviour and values for COF at RT (0.38–0.39) whereas, at 200 °C, the wear mechanism and values for COF were very different, according to the type and condition of the alloy (from 0.41 for Al80Mg10Si5Cu5 to 0.80 for AlSi9Cu3 alloy). COF values at 200 °C were higher because sliding wear is usually linked to two antagonistic effects: the wear process and the oxidation. As its known, the higher the test temperature, the higher the wear rates, with the wear rate not being proportional to the temperature, but increasing significantly around 200 °C for aluminium alloys, as the mechanisms of plastic deformation are dominant [79]. The delamination mechanism contribution (caused by the oxidation layer and more brittle phases broken and embedded into the matrix increasing the contact conditions [80]) to friction coefficient values at high temperatures to 200 °C is greater [81], as stronger atomic are formed between the aluminium alloy and the ball, with AlSi9Cu3 obtained values following previous works [23].

3.7. Wear surface analysis

Fig. 16 displays the 3D profiles of wear scars of as-cast, TT-Al80Mg10Si5Cu5 and as-cast AlSi9Cu3 alloys at different temperature conditions. In the case of the sample AlSi9Cu3 without the surface layer tested at 200 °C the employed scale is different from the rest to allow comparing the results.

The values for specific wear rates at the different temperatures are collected in Table 6.

As-cast Al80Mg10Si5Cu5 alloy with the surface layer showed the lowest values for the specific wear rate. At RT, the specific wear rate was 4.9×10^{-4} mm^3/N.m and 3.6×10^{-3} mm^3/N.m at 200 °C. In the case of the sample without the superficial layer, the value for specific wear rate was slightly higher, being 1.0×10^{-3} mm^3/N.m at RT and 4.4×10^{-3} mm^3/N.m at 200 °C. The surface layer contributed to increasing wear resistance, by presenting a higher hardness as well as a lower number of smaller and fragile eutectic intermetallic particles and defects. With the obtained values, it's expected to observe a mild wear mechanism at RT and 200 °C [53–56].

The TT-Al80Mg10Si5Cu5 alloys showed higher wear rate values. These samples have lower hardness values with more spherical phases. The fact that abrasion and adhesion wear mechanisms were increased contradicts one of the findings reported in the literature [59] but it is in accordance with the increase of abrasion and adhesion values with a decrease in hardness values in AlSiCu alloys with temperature [23]. The sample with the superficial layer showed a specific wear value of 1.1×10^{-3} mm^3/N.m at RT and 4.8×10^{-3} at 200 °C. At RT, the specific wear rate was 1.4×10^{-3} mm^3/N.m and 5.1×10^{-3} mm^3/N.m at 200 °C in the inner area. Samples without the surface layer showed similar but slightly superior values to those of samples with the surface layer, which can be related to the modification of the surface layer structure after the TT, showing a more similar structure to that of the inner area, but with a smaller number of defects and a slightly higher hardness, that could explain a slightly better resistance to wear in the surface layer area. In this case, it's also expected to observe a mild wear mechanism at RT and 200 °C [53–56].

AlSi9Cu3 alloy showed higher values for specific wear rates. At RT, the sample with the superficial layer had a specific wear value of 6.9×10^{-4} mm^3/N.m and 12.3×10^{-3} mm^3/N.m at 200 °C. The sample without the superficial layer showed a specific wear value of 1.6×10^{-3} mm^3/N.m at RT being around 57 % higher than the value of the Al80Mg10Si5Cu5 alloy without the surface layer, 44.8×10^{-3} mm^3/N.m at 200 °C, around 10 times higher than the value of Al80Mg10Si5Cu5. The obtained values at 200 °C are in accordance with the values obtained previously [23]. With the obtained values, it's expected to observe a mild-severe wear mechanism at RT and severe at 200 °C [53–56].

The newly developed Al80Mg10Si5Cu5 alloy in the as-cast state presented the lowest values for the specific wear rate at RT and in the as-cast and heat-treated state at 200 °C compared with the AlSi9Cu3 alloy.

3.8. Analysis of Al_2O_3 counter-ball

An analysis of the condition of the balls after the tests was conducted. In all cases, some material adhesion was detected. Table 7 displays the average results and deviation of the length, width, and thickness of each trace of adhered material at RT and 200 °C. (N.A. = Not Appreciated).

For better observation, the images of the counter-balls are shown

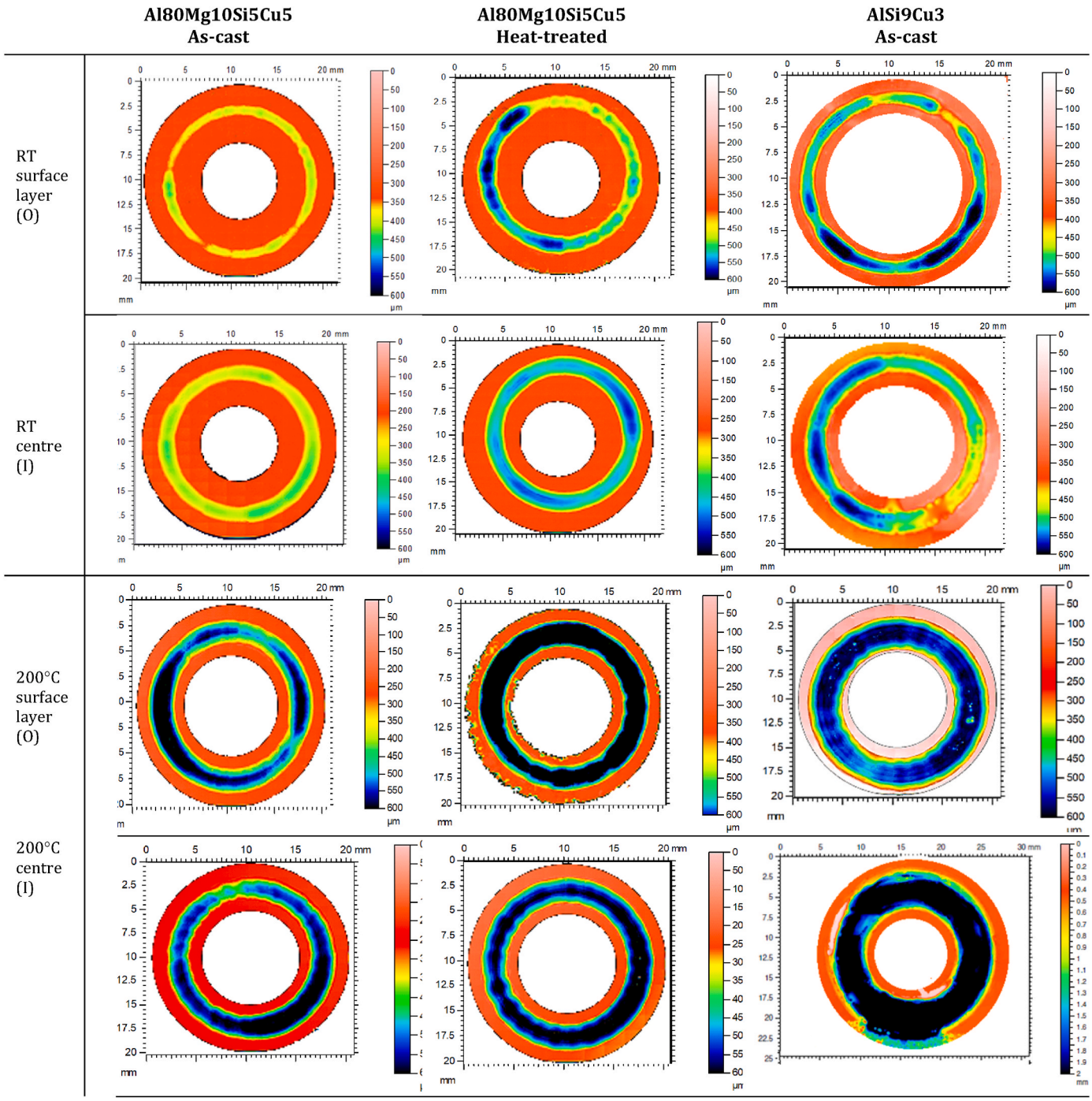

Fig. 16. Wear profiles at RT and 200 °C.

Table 6
Wear rate coefficients at RT and 200 °C.

REFERENCE	10^{-3}. K (mm^3/N.m)			
	RT		200 °C	
	S	I	S	I
Al80Mg10Si5Cu5 as-cast	0.5 ± 0.39	1.0 ± 0.19	3.6 ± 0.94	4.4 ± 0.96
Al80Mg10Si5Cu5 heat-treated	1.1 ± 0.43	1.4 ± 0.63	4.8 ± 0.33	5.1 ± 0.83
AlSi9Cu3 as-cast	0.7 ± 0.01	1.6 ± 0.16	12.3 ± 0.25	44.8 ± 1.23

Table 7
Measurements of material adhering to the ball.

Measures (mm)	Length	Width	Height
As-cast Al80Mg10Si5Cu at RT	2.00 ± 0.70	1.09 ± 0.15	N.A.
TT-Al80Mg10Si5Cu5 at RT	2.00 ± 0.26	1.25 ± 0.25	N.A.
As-cast AlSi9Cu3 at RT	2.17 ± 0.15	1.71 ± 0.38	N.A.
As-cast Al80Mg10Si5Cu at 200 °C	2.74 ± 0.37	1.37 ± 0.20	0.45 ± 0.08
TT-Al80Mg10Si5Cu5 at 200 °C	3.71 ± 0.21	1.77 ± 0.16	0.50 ± 0.11
As-cast AlSi9Cu3 at 200 °C	4.86 ± 1.17	4.57 ± 0.83	0.90 ± 0.41

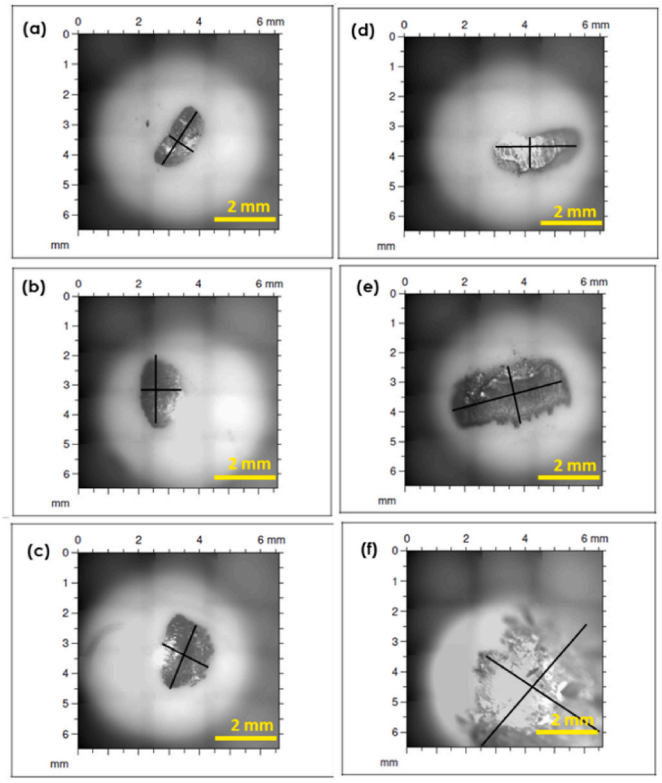

Fig. 17. Material track area after BOD tests. (a) As-cast Al80Mg10Si5Cu5 RT, (b) TT-Al80Mg10Si5Cu5 RT, (c) As-cast AlSi9Cu3 RT, (d) As-cast Al80Mg10-Si5Cu5 200 °C, (e) TT-Al80Mg10Si5Cu5 200 °C, (f) As-cast AlSi9Cu3 200 °C.

below. The area of adhered material can be observed in Fig. 17, while the resulting thickness in each case is shown in Fig. 18.

It can be easily observed that the adhered area is higher at 200 °C. Also, it was detected a higher thickness of adhered material at 200 °C, while at RT it was hardly detectable. The as-cast AlSi9Cu3 alloy tested at 200 °C showed the strongest adhesion, consisting of several layers up to nearly 1 mm and some adhesion was observed in TT-AlSi10Mg5Cu alloy. The alumina counter-balls didn't show any signal of wear, typical in steel counter-balls, which allows a better interpretation of results, with a minimal 3rd body wear from particle pull-out.

3.9. Analysis of wear surface at RT

The microstructural evolution of worn surfaces of the as-cast Al80Mg10Si5Cu5 alloy after the sliding wear test at RT is displayed in Fig. 19. The main wear mechanism was determined to be abrasion, characterized by plough lines in the same direction of the test direction produced by hard particle debris (principally Mg_2Si particles) [82]. There is also a plastic deformation of the matrix, as the matrix has a lower hardness and is ductile, penetrating the harder phases [42,83–86], and some oxidized particles. When comparing samples with the surface layer and without the surface layer (Fig. 19) the Al80Mg10Si5Cu5 as-cast alloy without the surface layer presented larger grooved regions and more pronounced plough lines. Also, where oxides are presented on the surface, the effect of the total wear and abrasion mechanism is lower [66] compared with the consequence of the formation of a mechanically mixed layer (MML) or transfer film (TF) [48,87,88]. The surface layer had higher hardness than the inner region, contributing to a decrease in the total wear. So, the results confirmed that the alloy acts under a mild wear regime.

In the analysis by SEM + EDS, it was observed that within the aluminium matrix (Point 1) some oxidized particles (Point 2) with a percentage of up to 40 % oxygen were detected. During the test, the

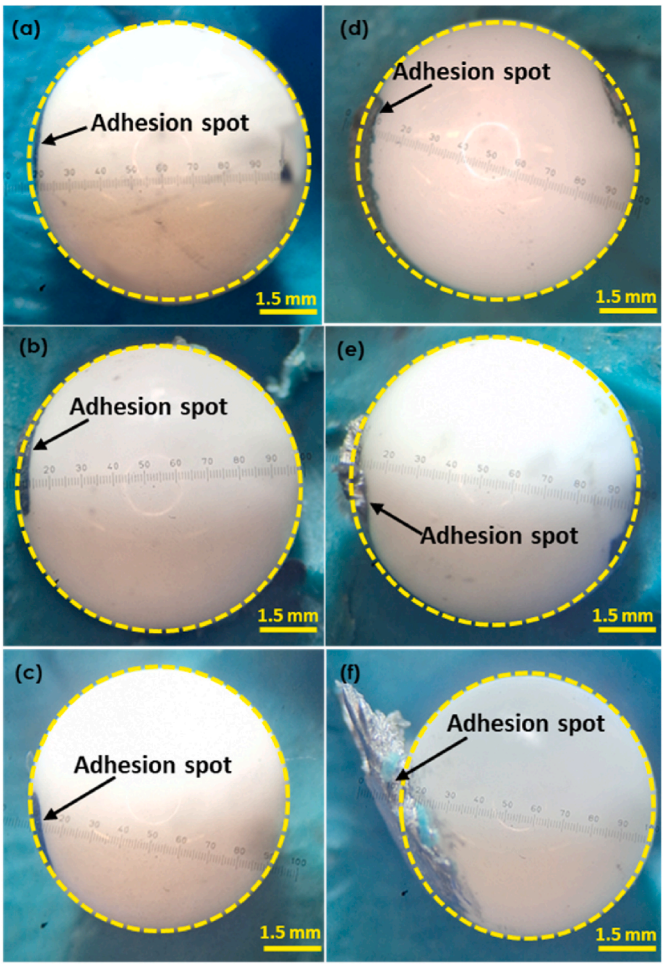

Fig. 18. Material track thickness determination at RT: (a) As-cast Al80Mg10-Si5Cu5 RT, (b) TT-Al80Mg10Si5Cu5 RT, (c) As-cast AlSi9Cu3 RT, and at 200 °C: (d) As-cast Al80Mg10Si5Cu5, (e) TT-Al80Mg10Si5Cu5, (f) As-cast AlSi9Cu3.

asperities joints and surface material break up, and they form oxidized debris particles that are compacted back again into the matrix. While larger and primary Mg_2Si phases are generally detached from the track, eutectic phases of Mg_2Si (point 3) and Cu-rich intermetallics (Point 4) are supposed to remain embedded in the matrix. Table 8 collects the approximative chemical composition of the analyzed points.

The microstructural evolution of worn surfaces of TT-Al80Mg10Si5Cu5 alloy after the sliding wear test at RT is displayed in Fig. 20. Abrasion was again the main wear mechanism [86]. Also, regions with plastic deformation over the plough lines on the track were arbitrarily presented, linked to the higher ductility and lower hardness values of the alloy in comparison to the as-cast state. The surface wear presented an area with debris and white zones near the ploughs, probably because of increased abrasion compared with as-cast Al80Mg10-Si5Cu5 alloy samples. When comparing samples with the surface layer and without the surface layer (Fig. 20), the TT-Al80Mg10Si5Cu5 alloy without the surface layer presented more roughened grooves and ploughed regions. The surface layer, by presenting higher hardness values, contributes to a decrease in the total wear, showing an abrasion mechanism with fewer plough lines over the surface grooves and a smaller number of cracks. The increased abrasion area confirms the higher values of wear rate obtained in the tests, probably related to the difference in the obtained microstructure after the heat treatment. The results confirmed that the alloy acts under a mild wear regime but with more cracks in the wear track.

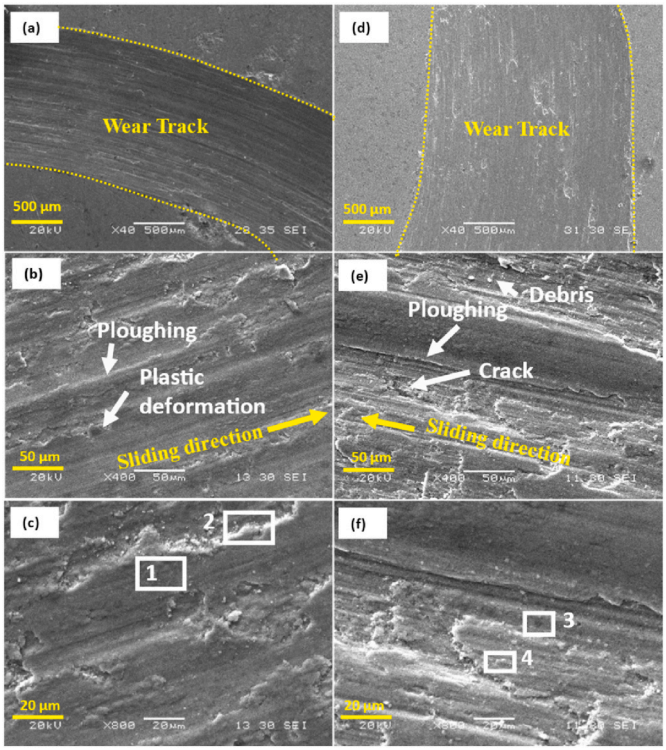

Fig. 19. SEM images of worn surface tested at RT for as-cast Al80Mg10Si5Cu5. (a), (b) and (c) = With surface layer at the magnification of×40, ×400 and x800. (d), (e) and (f) = Without surface layer at the magnification of×40, ×400 and x800.

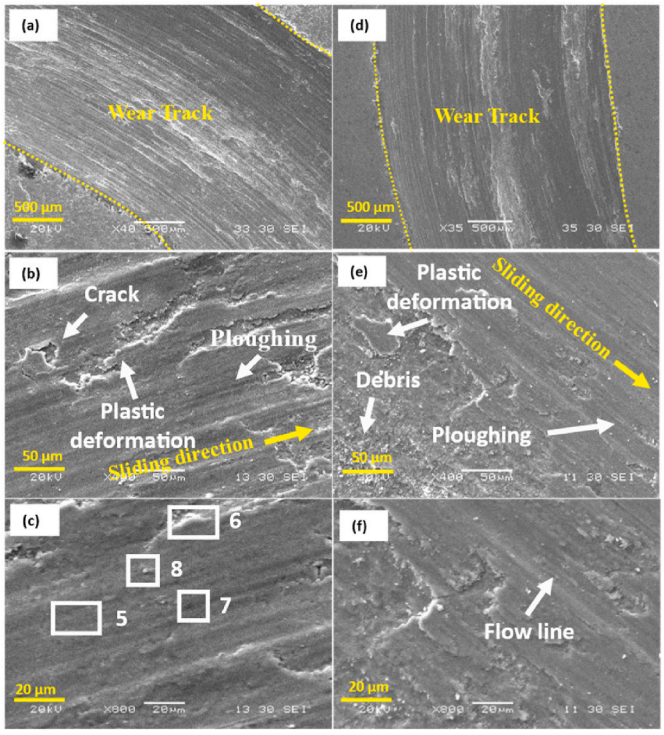

Fig. 20. SEM images of worn surface tested at RT for heat-treated Al80Mg10Si5Cu5. (a), (b) and (c) = With surface layer at the magnification of×40, ×400 and x800. (d), (e) and (f) = Without surface layer at the magnification of×40, ×400 and x800.

Table 8
Chemical wt.% composition of analyzed point.

Elements	Point 1	Point 2	Point 3	Point 4
Al	80.6	47.0	0.3	65.4
Mg	9.6	7.0	53.2	10.8
Si	4.1	3.1	28.6	0.9
Cu	5.7	2.7	–	21.6
O	–	40.3	9.1	1.4

Table 9
Chemical wt.% composition of analyzed points.

Elements	Point 5	Point 6	Point 7	Point 8
Al	75.8	48.6	37.4	62.1
Mg	11.8	6.1	32.5	6.7
Si	6.5	2.9	21.3	1.0
Cu	6.0	3.0	1.2	28.6
O	–	39.5	7.7	1.7

When microstructures were analyzed in TT-Al80Mg10Si5Cu5 alloy by EDS and phases estimated, it was observed that within the aluminium matrix (Point 5), oxidized areas at the edges of the ploughing areas (Point 6) with a percentage of 39 % of oxygen were detected, corresponding to the white lines observed in the wear track. In this case, eutectic phases of Mg_2Si (point 7) and Cu-rich intermetallics (Point 8) remained embedded in the matrix. Table 9 collects the approximative chemical composition of analyzed points.

The microstructural evolution of worn surfaces of as-cast AlSi9Cu3 alloy after the test at RT is displayed in Fig. 21. The AlSi9Cu3 alloy presented abrasion as the main mechanism, but with some areas with ductile delamination [86–89]. The surface wear presented a large number of debris in different directions as a result of increased abrasion, in comparison with Al80Mg10Si5Cu5 alloy samples. It could be justified because it's the alloy with the lowest hardness and the highest wear rate, including the higher number of hard precipitates, including iron phases. When comparing the samples with the superficial layer and without the surface layer (Fig. 21), the alloy without the surface layer presented an increased delaminated area. The surface layer, by presenting better hardness properties and fewer defects, contributes to a decrease in the total wear and therefore showing less abrasive and delaminated areas. The alloy showed mild wear but with some signs of severe wear.

EDS analysis of AlSi9Cu3 alloy showed that the aluminium matrix (point 9) was partially oxidized with around 32 % of oxygen in white colour particles (point 10). In the delamination mechanism, the layers that are created in the aluminium matrix get oxidized, and asperities are created. These asperities break up and get formed into debris particles, that are compacted back into the matrix. The rest of the phases rich in Cu, probably Al_2Cu (point 11) and silicon (point 12) kept embedded. Also, iron intermetallic particles (point 13) were detected (see Table 10). The compact-shaped iron intermetallics tend to develop surface and subsurface microcracks, forming a rough interface with the matrix, which reduces the likelihood of decohesion at the interface. Conversely, needle-like iron compounds (β-Fe phase) are hard and brittle, making them prone to fracture compared to the eutectic Si particles or the α-Al matrix, resulting in the propagation of microcracks that eventually lead to macrocracks [24].

3.10. Analysis of wear surface at 200 °C

The microstructural evolution of worn surfaces of as-cast Al80Mg10Si5Cu5 alloy at 200 °C is displayed in Fig. 22.

The main wear mechanism was abrasion, characterized by the formation of scratches on the worn surface in the sliding direction with some debris and slight plastic deformation of the aluminium matrix. The presence of higher plastic deformation in comparison to the as-cast Al80Mg10Si5Cu5 alloy tested at RT could be related to the increase in

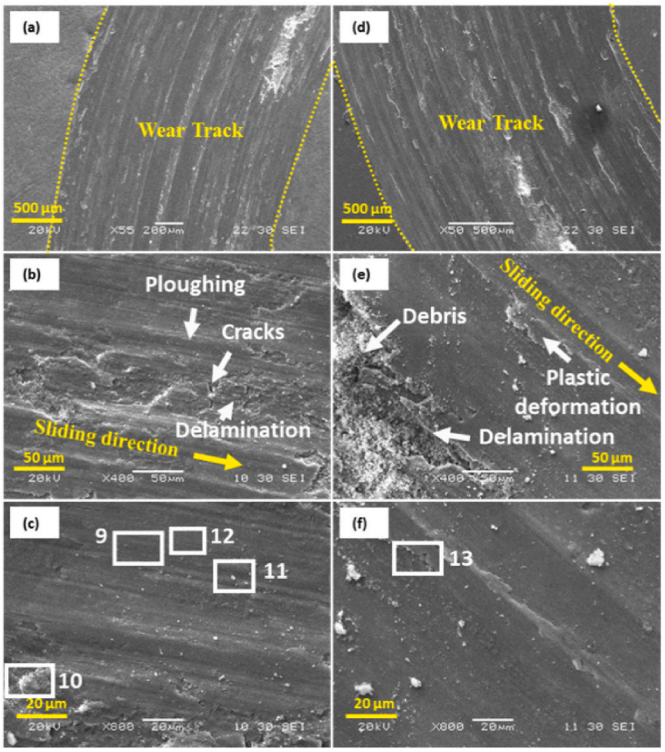

Fig. 21. SEM images of worn surface tested at RT for as-cast AlSi9Cu3. (a), (b) and (c) = With surface layer at the magnification of×40, ×400 and x800. (d), (e) and (f) = Without surface layer at the magnification of×40, ×400 and x800.

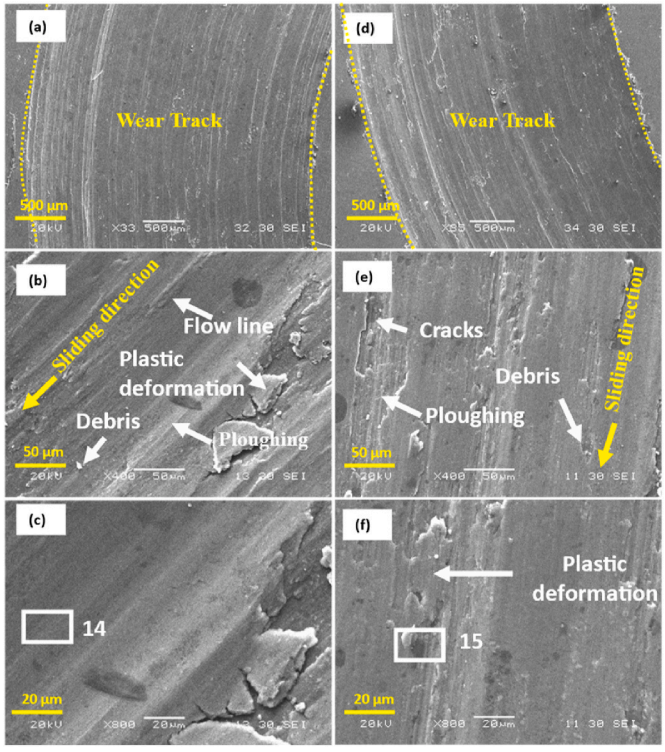

Fig. 22. SEM images of worn surface for as-cast Al80Mg10Si5Cu5. (a), (b) and (c) = With surface layer at the magnification of×40, ×400 and x800. (d), (e) and (f) = Without surface layer at the magnification of×40, ×400 and ×800 at 200 °C.

Table 10
Chemical wt.% composition of analyzed points.

Element	Point 9	Point 10	Point 11	Point 12	Point 13
Al	85.7	59.0	62.9	52.4	65.9
Si	7.6	6.1	5.3	40.2	16.9
Cu	2.2	1.9	31.8	2.0	0.9
Mn	–	–	–	–	1.8
Fe	0.7	0.8	–	–	14.5
O	3.8	32.3	–	5.4	–

Table 11
Chemical wt.% composition of analyzed points.

Element	Point 14	Point 15
Al	64.4	55.6
Mg	6.9	10.7
Si	5.1	3.8
Cu	2.9	2.5
O	19.9	27.4

the temperature. Some delaminated areas were identified. Also, the presence of rounded debris is remarkable. When comparing samples with and without the superficial surface layer (Fig. 22), the sample with the surface layer presented fewer regions with plastic deformation, resulting in decreased wear, probably because the surface layer presented a higher hardness and fewer defects. The results confirmed that the alloy acts under a mild wear regime but with more plastically deformed areas than at RT.

Al80Mg10Si5Cu5 alloy microstructures was analyzed by EDS and phases were estimated. It was observed a similar microstructure to the one at RT and with and without surface layer. However, some dark-grey particles were observed (Points 14 and 15), corresponding to the oxidized particles of the aluminium matrix. These oxides could be formed in the test at 200 °C, where samples were tested without a protective atmosphere, oxidizing the sample surfaces. Table 11 collects the approximative chemical composition of the analyzed points.

The microstructural evolution of worn surfaces of the TT-Al80Mg10Si5Cu5 alloy after the test at 200 °C is displayed in Fig. 23.

The main wear mechanism was abrasion, with some ductile delaminated areas with extender crack propagation than in as-cast samples. As a results of severely plastically deformed layers, adhesion can also occur. However, adhesion was identified as a secondary mechanism [90]. The presence of rounded debris and delaminated areas is remarkable being abrasion the predominant wear mechanism. When comparing samples with and without the superficial surface layer.

When comparing the samples with and without the surface layer (Fig. 23), the sample with the surface layer presented less abrasion and more delaminated areas, which can be correlated with the observed higher COF value.

When microstructures were analyzed by EDS, the material was quite similar in the as-cast and in the TT sample. Due to wear, the layers that are being created in the aluminium matrix are oxidized, and finally, asperities are created. These asperities will break up and will be transformed into debris particles which are compacted back into the matrix. Remarkably, the Al_2Cu phase in the as-cast Al80Mg10Si5Cu5 alloy is not detected at 200 °C in the TT samples. This could also justify a higher wear rate at 200 °C on TT samples, because of the significance of the Al_2Cu phase as a wear-resistant element, in line with previous findings in Al-Si-Cu-Mg alloys, where the formation of Al_2Cu and Q ($Al_XMg_5Cu_4Si_4$) phases promotes the use of aluminium alloys at elevated temperatures [91–94]. On the contrary, TT-Al80Mg10Si5Cu5 alloy presented the same microstructure at 200 °C. In these samples, the wear mechanism has moved from mild to mild-severe wear, so TT is not desirable for the developed alloy for wear applications.

The microstructural evolution of worn surfaces of the as-cast AlSi9Cu3 alloy after the sliding wear test at 200 °C is displayed in

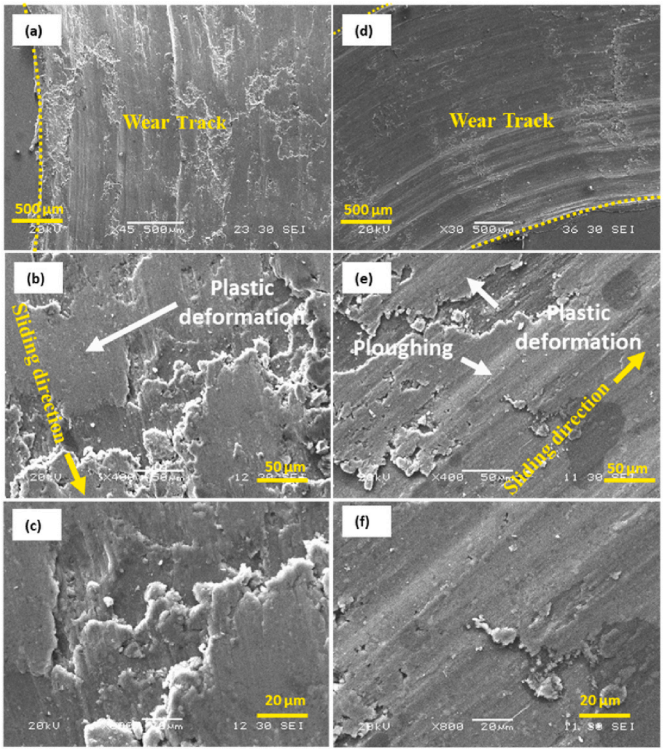

Fig. 23. SEM images of worn surface for TT-Al80Mg10Si5Cu5. (a), (b) and (c) = With surface layer at the magnification of×40, ×400 and x800. (d), (e) and (f) = Without surface layer at the magnification of×40, ×400 and ×800 at 200 °C.

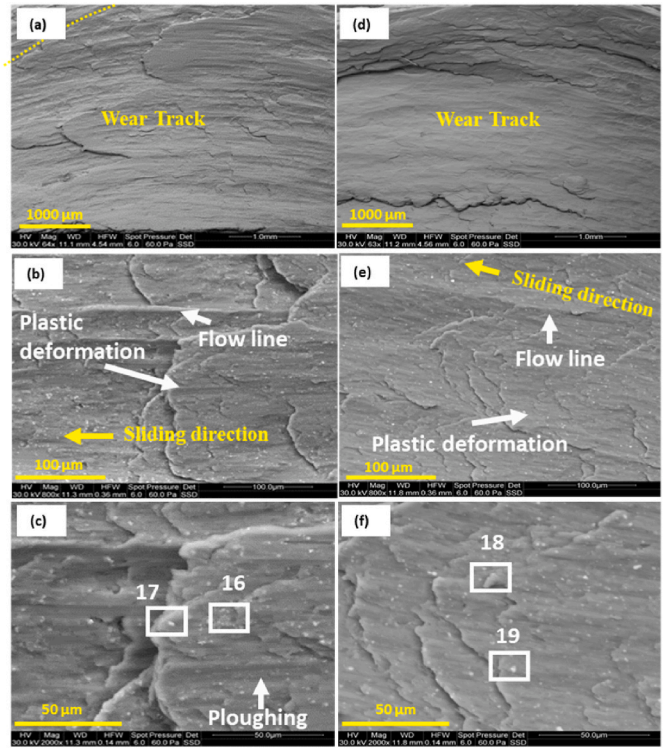

Fig. 24. SEM images of worn surface for as-cast AlSi9Cu3. (a), (b) and (c) = With skin at the magnification of×40, ×400 and x800. (d), (e) and (f) = Without skin at the magnification of×40, ×400, ×800 at 200 °C.

Fig. 24.

AlSi9Cu3 alloy in the as-cast condition presented a combination of some areas with abrasion and predominant ductile delamination wear mechanisms at 200 °C. Additionally, it was the one that exhibited the greatest plastic deformation. The wear surface presented regions with pronounced delaminated areas. As a result of severely plastically deformed layers, adhesion can also occur, being delamination one of the adhesion wear mechanisms [90]. The sliding direction and wear tracks were not discernible in the sample without the surface layer. The material removal resulted from the delamination of subsurface layers. When a continuous mechanically mixed layer (MML) or TF is formed, the wear rate decreases in comparison with non-continuous MMLs [95], and in the analyzed samples a near-continuous MML was observed. Unlike the Al80Mg10Si5Cu5 alloy, the worn surface of AlSi9Cu3 presented highly plastically deformed material as indicated in Fig. 24. It can be observed that the wear mechanism promotes principally ductile delamination. The results confirmed that the alloy acts under a severe wear regime.

When microstructures were analyzed by EDS, the aluminium matrix didn't show oxidized particles. This could be related to the highest value of COF at 200 °C, and delamination acting as the main wear mechanism. It was confirmed that the aluminium matrix was delaminated and some intermetallics were presented in the studied area. These precipitates had a polygonal shape, being correlated with the AlSi eutectic phase (point 16 and point 18) and with Fe and Cu-rich particles (point 17 and point 19). The presence in the track area of small polygonal phases could reduce the abrasion effect of bigger or acicular intermetallic phases, which could be correlated with the small ploughings on the test surface. Table 12 collects the approximative chemical composition of the analyzed points.

3.11. Subsurface analysis

Following there are shown the cross-section micrographs of the wear tracks tested at RT (Fig. 25) and 200 °C (Fig. 26) observed by optical microscopy (OM). As-cast Al80Mg10Si5Cu5 alloy, tested at RT exhibited smaller intermetallic phases, particularly Mg_2Si, on the contact surface area compared to the rest of the area. The various phases have been determined by the SEM + EDS, as detailed in section 3.9. The amount of material removed from the contact surface due to the abrasion as the principal wear mechanism is clearly at higher magnifications. The deformation of the wear track resulting from compressive forces showed cracked Mg_2Si phases and layered debris, due to hard asperities induced microcracking [86]. In the case of as-cast AlSi9Cu3, tested at RT, the deformed contact surface was smaller, but the presence of cracks was more noticeable in some regions due to signs of ductile delamination. Although abrasion was the principal wear mechanism a higher degree of delamination was observed [86,87], with some small superficial cracks. Additionally, on the contact surface, the silicon particles exhibited a more globular shape, in contrast to the more laminar shape observed on the inner surface. So, the subsurface analysis showed that the wear rate of Al80Mg10Si5Cu5 alloy is mild and the AlSi9Cu3 wear rate is mild but some small severe wear areas.

The as-cast Al80Mg10Si5Cu5 alloy, tested at 200 °C, exhibited a smaller deformed contact area compared to the alloy tested at RT. Some

Table 12
Chemical wt.% composition of analyzed points.

Element	Point 16	Point 17	Point 18	Point 19
Al	83.9	76.8	84.7	71.7
Si	9.5	5.8	10.4	14.2
Cu	2.8	15.7	2.3	12.7
Fe	1.7	0.5	0.9	0.4
Mn	0.6	–	–	–
O	1.5	1.2	1.7	1.1

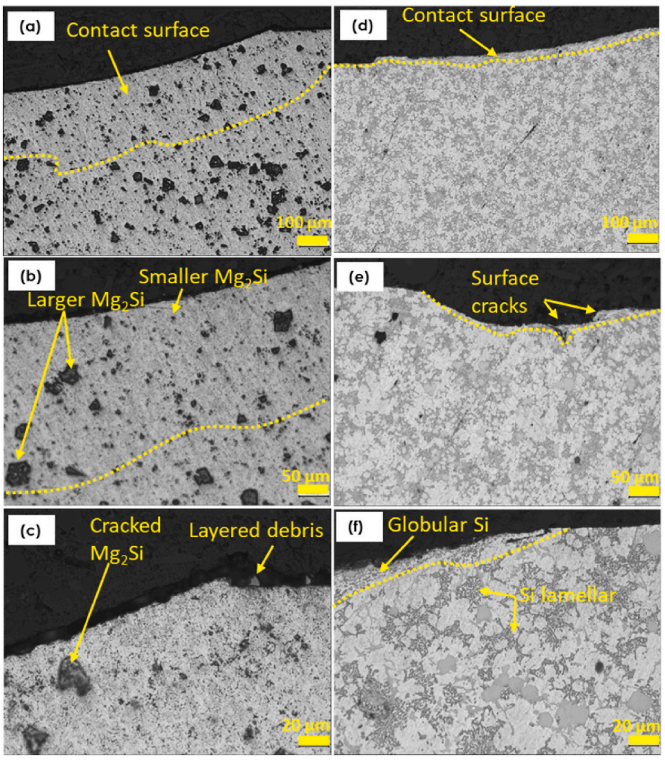

Fig. 25. OM cross-section micrographs of the wear tracks tested at RT for as-cast Al80Mg10Si5Cu5 at ×100 (a), ×200 (b), and ×500 (c) and as-cast AlSi9Cu3 at ×100 (d), ×200 (e) and ×500 (f).

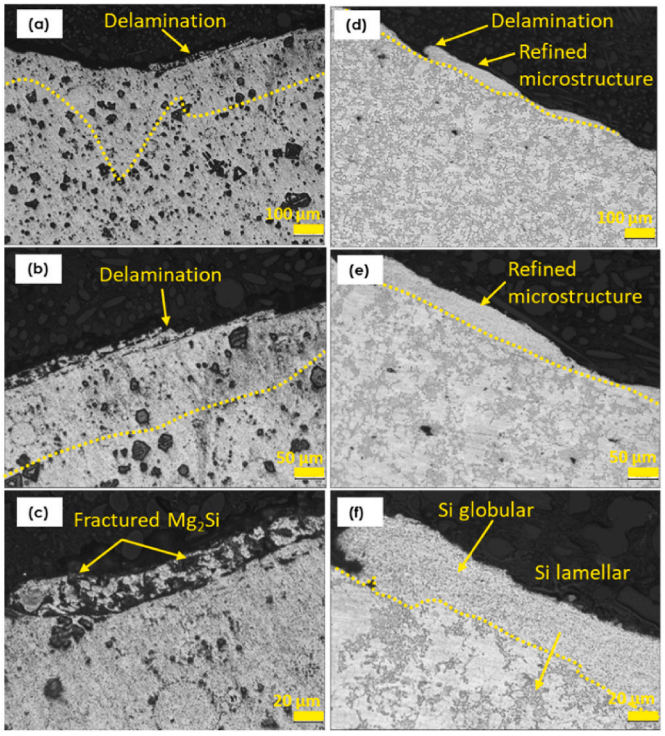

Fig. 26. OM cross-section micrographs of the wear tracks tested at 200 °C for as-cast Al80Mg10Si5Cu5 at ×100 (a), ×200 (b), ×500 (c), as-cast AlSi9Cu3 at ×100 (d), ×200 (e) and ×500 (f).

delaminated areas with fractured Mg_2Si particles were visible on the contact surface, indicating that in addition to abrasion as the principal wear mechanism delamination wear also occurred due to the formation of sublayers [85,86]. In the case of the as-cast AlSi9Cu3 tested at 200 °C, a thicker layer with a finer microstructure, ranging from 10 µm to 40 µm thick, was detected compared to the sample tested at RT, indicating more severe wear. The increase in temperature promotes an increase in the oxidation rate of these alloys [96] as it was determined in section 3.10. The fractured/fragmented oxide layer and the wear debris of contact surfaces could cause the formation of tribochemical reactions [85], and as a consequence, a mechanically mixed layer (MML) or transfer film (TF) [87,88,96]. If these transfer films form a continuous layer, wear rate is reduced [95]. The analysis showed that Al80Mg10-Si5Cu5 alloy combines mild and some small severe wear rate areas at 200 °C and AlSi9Cu3 a severe wear rate.

4. Conclusions

This paper has comprehensively investigated the friction and wear properties of a new Al80Mg10Si5Cu5 cast alloy and compared them with the AlSi9Cu3 cast alloy at RT and at 200 °C in as-cast and thermal treated state, including the effect of the external skin of die-cast parts on wear. The conclusions are as follows:

(1) →The novel Al80Mg10Si5Cu5 alloy developed for HPDC is characterized by enhanced wear properties compared to the standard AlSi9Cu3 alloy at RT (+50 % reduction in wear rate). This improvement is attributed to the hardness of the surface and subsurface, but also to the type and morphology of the microstructure in the new alloy, with abrasion as the main wear mechanism. AlSi9Cu3 alloy showed abrasion accompanied by some ductile delamination with a higher specific wear rate. At RT, Al80Mg10Si5Cu5 alloy showed a mild wear rate and AlSi9Cu3 mild wear but with some signs of severe wear.

(2) →At 200 °C, the wear rate and COF values are higher. Al80Mg10Si5Cu5 alloy in the as-cast condition with the surface layer presented again the lowest wear rate with abrasion wear, showing mild wear. TT-Al80Mg10Si5Cu5 alloy exhibited abrasion along with a predominant secondary ductile delamination wear mechanism in comparison to as cast Al80Mg10Si5Cu5 alloy, showing mild wear but with some signs of severe wear. As-cast AlSi9Cu3 alloy exhibited the highest wear rates (x10 times reduction in wear rate) and predominantly showed the ductile delamination mechanism, showing severe wear.

(3) →Samples with the surface layer presented lower COF values and specific wear rates, because of higher hardness, better microstructure, and reduced quality defects. Avoiding the machining of HPDC cast parts could improve in-service performance under wearing conditions.

(4) → The newly developed alloy shows promise as a cost-effective and low CO_2 alternative for aluminium drum brakes. It offers advantages due to its performance properties obtained from secondary aluminium alloys, which are also lighter than iron which potentially enhance fuel efficiency. Additionally, the HPDC process used for its production results in reduced cycle times among other advantages.

Funding

This work has been partially funded by the Basque Government through the ELKARTEK KK-2020_00047 (CEMAP), KK-2022_00082 (MINERVA), and KK-2023/00020 (DESGAS).

CRediT authorship contribution statement

Ester Villanueva: Writing – original draft, Methodology,

Investigation. **Iban Vicario:** Writing – original draft, Supervision, Project administration, Methodology, Investigation. **Joseba Albizuri:** Validation, Supervision, Project administration, Investigation. **Gurutze Arruebarrena:** Writing – review & editing, Validation, Investigation. **Teresa Guraya:** Writing – review & editing, Validation, Investigation.

Declaration of competing interest

The authors declare the following financial interests/personal relationships which may be considered as potential competing interests:

Joseba Albizuri has patent #EP23383372.2 pending to UPV and Tecnalia. If there are other authors, they declare that they have no known competing financial interests or personal relationships that could have appeared to influence the work reported in this paper.

Data availability

Data will be made available on request.

References

[1] P. Sharma, V.K. Dwivedi, S.P. Dwivedi, Development of high entropy alloys: a review, Mater. Today: Proc. 43 (1) (2021) 502–509, https://doi.org/10.1016/j.matpr.2020.12.023.

[2] S. Salifu, P.A. Olubambi, Effects of fabrication techniques on the mechanical properties of high entropy alloys: a review, Int. J. Lightweight Mater Manufact (2023) 13–53, https://doi.org/10.1016/j.ijlmm.2023.08.001.

[3] D. Lehmhus, Advances in metal casting technology: a review of state of the art, challenges and trends—Part I: changing markets, changing products, Metals 12 (2022) 1959, https://doi.org/10.3390/met12111959.

[4] Applications – Chassis & Suspension, Brake System; the Aluminium Automotive Manual, European-Aluminium Association, 2011. Available online: https://european-aluminium.eu/wp-content/uploads/2022/11/aam-applications-chassis-suspension-5-brake-system.pdf.

[5] S.A. Awe, A. Thomas, The prospects of lightweight SICAlight discs in the emerging disc brake requirements, Eurobrake (2020) 1–8.

[6] M.N. Ervina, H.J. Kong, C.K. Kok, Review: effect of alloying element on Al-Si alloys, Adv. Mater. Res. 845 (2013) 355–359. https://doi.org/10.4028/www.scientific.net/AMR.845.355.

[7] S. Sharma, T. Nanda, O.P. Pandey, Investigation of T4 and T6 heat treatment on the wear properties of sillimanite reinforced LM30 aluminium alloy composites, Wear (2019) 426–427, https://doi.org/10.1177/13506501211036543, 27–36.

[8] Y. Chen, Q. Hu, S. Pan, H. Zhang, H. Liu, B. Zhu, X. Liu, W. Liu, Influences of Cu content on the microstructure and strengthening mechanisms of Al-Mg-Si-xCu alloys, Metals 9 (5) (2019) 524, https://doi.org/10.3390/met9050524.

[9] J. Zhang, A.T. Alpas, Transition between mild and severe wear in aluminium alloys, Acta Mater. 45 (1997) 513–528, https://doi.org/10.1016/S1359-6454(96)00191-7.

[10] A. Pauschitz, M. Roy, F. Franek, Mechanisms of sliding wear of metals and alloys at elevated temperatures, Tribol. Int. 41 (7) (2008) 584–602, https://doi.org/10.1016/j.triboint.2007.10.003.

[11] D. Culliton, A.J. Betts, D. Kennedy, Impact of intermetallic precipitates on the tribological and/or corrosion performance of cast aluminium alloys: a short review, Int. J. Cast Metals Res. 26 (2013) 65–71, https://doi.org/10.1179/1743133612Y.0000000038.

[12] K.Y. Lee, S.L. Lee, C.T. Wu, W.C. Chen, J.C. Lin, Effects of T6 heat treatment on thermal stability and wear behaviour of Al-12.5Si-4.5Cu-1.0Mg alloy, Mater. Sci. Technol. 28 (2012) 639–643, https://doi.org/10.1179/1743284711Y.0000000057.

[13] P.K. Dinesh, S. Darius, Aluminium-Silicon based Metal Matrix Composites for brake rotor applications: a review, Eng. Res. Express 5 (2023) 022002, https://doi.org/10.1088/2631-8695/accdb6.

[14] S. Kumar, R. Pandey, R. Panwar, O.P. Pandey, Effect of particle size on wear of particulate reinforced aluminum alloy composites at elevated temperatures, J. Mater. Eng. Perform. 22 (11) (2013) 1–12, https://doi.org/10.1007/s11665-013-0642-8.

[15] M.R. Schütte, J. Ehrich, D. Linsler, S. Hanke, Effects of microstructure modification by friction surfacing on wear behaviour of Al alloys with different Si contents, Materials 15 (2022) 1641, https://doi.org/10.3390/ma15051641.

[16] B.E. Slattery, A. Edrisy, T. Perry, Investigation of wear induced surface and subsurface deformation in a linerless Al–Si engine, Wear 269 (3–4) (2010) 298–309, https://doi.org/10.1016/j.wear.2010.04.012.

[17] P.K. Yadav, G. Dixit, S. Dixit, V.P. Singh, S.K. Patel, R. Purohit, B. Kuriachen, Effect of eutectic silicon and silicon carbide particles on high stress scratching wear of aluminium composite for various testing parameters, Wear 482–483 (2021) 3–13, https://doi.org/10.1016/j.wear.2021.203921.

[18] S. Aksoy, F. Kabakc, M. Acarer, H. Düzcükoğlu, E. Ünüvar, F. Fındık, Effect of Mg addition on microstructure and mechanical properties of AlSi12 alloy produced by high-pressure casting method, Ind. Lubric. Tribol. 75 (1) (2023) 27–35, https://doi.org/10.1108/ILT-10-2021-0410.

[19] K. Kanayo, T. Moyosore, P. Apata, Corrosion and wear behaviour of Al–Mg–Si alloy matrix hybrid composites reinforced with rice husk ash and silicon carbide, J. Mater. Res. Technol. 3 (1) (2014) 9–16, https://doi.org/10.1016/j.jmrt.2013.10.008.

[20] B. Chandra Mouli, D. Naresh, K.S.J. Prakash, A. Bala Krishna, Effect of copper content on wear properties of aluminium alloy, J. Chem. Pharmaceut. Sci. 10 (2) (2017) 1059–1071.

[21] M.S. Prabhudeva, V. Auradi, K. Venkateswarlu, N.H. Siddalingswamy, S.A. Kori, Influence of Cu addition on dry sliding wear behaviour of A356 alloy, Procedia Eng. 97 (2014) 1361–1367, https://doi.org/10.1016/j.proeng.2014.12.417.

[22] N. Kashimat, S. Sharma, R. Nayak, K.B. Manjunathaiah, M. Shettar, G. M. Chennegowda, Experimental investigation of mechanical property and wear behaviour of T6 treated A356 alloy with minor addition of copper and zinc, J. Compos. Sci. 7 (2023) 149, https://doi.org/10.3390/jcs7040149.

[23] G. Timelli, A. Fabrizi, S. Vezzù, A. De Mori, Design of wear-resistant diecast AlSi9Cu3(Fe) alloys for high-temperature components, Metals 10 (55) (2020) 1–16, https://doi.org/10.3390/met10010055.

[24] G. Timelli, Evolution of sludge particles in secondary die-cast aluminum alloys as function of Fe, Mn and Cr contents, Mater. Chem. Phys. 153 (2015) 168–179, https://doi.org/10.1016/j.matchemphys.2014.12.050.

[25] M.L. Rahaman, L. Zhang, An investigation into the friction and wear mechanisms of aluminium high silicon alloy under contact sliding, Wear 376–377 (2017) 940–946, https://doi.org/10.1016/j.wear.2016.10.026.

[26] J. Zhu, Z. Luo, S. Wu, H. Yan, The effect of Sr on the microstructure and wear properties of AlSi5Cu1Mg alloy, Adv. Mech. Eng. 10 (12) (2018) 1–10, https://doi.org/10.1177/1687814018819536.

[27] Q. Zhang, S. Wei, J. Gu, M. Qi, High-temperature dry sliding wear behavior of Al–12Si–CuNiMg alloy and its Al2O3 fiber-reinforced composite, Met. Mater. Int. 9 (2021) 1–11, https://doi.org/10.1007/s12540-020-00654-4.

[28] C. Fiell, P. Fiell, Friction, lubrication and wear technology, ASM Handb. 18 (2017) 1599–1617.

[29] N.P. Suh, The delamination theory of wear, Wear 25 (1) (1973) 111–124, https://doi.org/10.1016/0043-1648(73)90125-7.

[30] N.P. Suh, E.P. Abrahamson, A.P.L. Turner, Further investigation of the delamination theory of wear, J. Lubric. Technol. 96 (1974) 631–637, https://doi.org/10.1115/1.3452511.

[31] C.R. Raghavgendra, Analysis of tribological behavior, pin temperature, and surface roughness of a brake pad material with nano coating, Tribology 197 (2024) 109727, https://doi.org/10.1016/j.triboint.2024.109727.

[32] C.R. Raghavendra, S. Basavarajappa, I. Sogalal, Sliding wear behaviour of Ni-α-Al2O3 nano composite coating at elevated temperatures, Colloid Interface Sci. Commun. 27 (2018) 18–25, https://doi.org/10.1016/j.colcom.2018.09.003.

[33] L. Wang, Y. He, J. Zhou, J. Duszczyk, Effect of temperature on the frictional behaviour of an aluminium alloy sliding against steel during ball-on-disc tests, Tribol. Int. 43 (2010) 299–306, https://doi.org/10.1016/j.triboint.2009.06.009.

[34] G. Rajaram, S. Kumaran, T. Srinivasa Rao, High temperature tensile and wear behaviour of aluminum silicon alloy, Mater. Sci. Eng. 528 (2010) 247–253, https://doi.org/10.1016/j.msea.2010.09.020.

[35] M. Vilaseca, S. Molas, D. Casellas, High-temperature tribological behaviour of tool steels during sliding against aluminium, Wear 272 (1) (2011) 105–109, https://doi.org/10.1016/j.wear.2011.07.007.

[36] L. Ceschini, A. Morri, S. Toschi, S. Johansson, S. Seifeddine, Microstructural and mechanical properties characterization of heat treated and overaged cast A354 alloy with various SDAS at room and elevated temperature, Mater. Sci. Eng. 648 (2015) 340–349, https://doi.org/10.1016/j.msea.2015.09.072.

[37] V. Abouei, H. Saghafian, S.G. Shabestari, M. Zarghami, Effect of Fe-rich intermetallics on the wear behavior of eutectic Al-Si piston alloy (LM13), Mater. Des. 31 (2010) 3518–3524, https://doi.org/10.1016/j.matdes.2010.02.015.

[38] R. Taghiabadi, H.M. Ghasemi, S.G. Shabestari, Effect of iron-rich intermetallics on the sliding wear behaviour of Al-Si alloys, Mater. Sci. Eng. 490 (2008) 162–170, https://doi.org/10.1016/j.msea.2008.01.001.

[39] M. Dhiman, D.K. Dwivedi, R.S. Sehgal, I.K. Bhat, Effect of iron (wt.%) on adhesive wear response of Al-12Si-1Cu-0.1Mg alloy in dry sliding conditions, Trans. Indian Inst. Met. 61 (2008) 451–456.

[40] C.R. Raghavgendra, K.P. Jhansilakshmi, Study on pin temperature and wear behaviour of plasma sprayed Ni-Cr coatings with nano Al2O3 particle, Int. J. Surf. Eng. Coating. 102 (2024) 215–228, https://doi.org/10.1080/00202967.2024.2326388.

[41] C.R. Raghavgendra, Relationship between flash temperature and wear characteristics in Ni-nano Al2O3 coating, J. Adhes. Sci. Technol. 36 (2021) 1–16, https://doi.org/10.1080/01694243.2021.2010880.

[42] E.C. Talibouya, M. Rosa, P. Sérgio, R. Martins, M.P. Martins da Cruz, V. Ferreira, Investigation of the effects of skewness Rsk and kurtosis Rku on tribological behavior in a pin-on-disc test of surfaces machined by conventional milling and turning processes, Mater. Res. 24 (2) (2021) 1–14, https://doi.org/10.1590/1980-5373-MR-2020-0435.

[43] M. Krbata, M. Eckert, J. Majerik, I. Barenyi, Wear behaviour of high strength tool steel 90MnCrV8 in contact with Si3N4, Metals 10 (756) (2020), https://doi.org/10.3390/met1006075.

[44] M. Stembalskin, P. Pres, W. Skoczynski, Determination of the friction coefficient as a function of sliding speed and normal pressure for steel C45 and steel 40HM, Arch. Civ. Mech. Eng. 13 (2013) 444–448, https://doi.org/10.1016/j.acme.2013.04.010.

[45] J. Salguero, J.M. Vazquez-Martinez, I. Del Sol, M. Batista, Application of pin-on-disc techniques for the study of tribological interferences in the dry machining of A92024-T3 (Al-Cu), Alloys. Mater. 11 (7) (2018) 1236, https://doi.org/10.3390/ma11071236, 3-9.

[46] R.N. Rao, S. Das, D.P. Mondal, G. Dixit, S.L.T. Devi, Dry sliding wear maps for AA7010 (Al–Zn–Mg–Cu) aluminium matrix composite, Tribol. Int. 60 (2013) 77–82, https://doi.org/10.1016/j.triboint.2012.10.007.

[47] B.M. Satish, B.P. Shivakumar, M.B. Hanamantraygouda, Wear behaviour of hot forged SiC reinforced aluminium 6061Composite materials, Aust. J. Mech. Eng. 20 (2020) 425–432, https://doi.org/10.1080/14484846.2020.1714353.

[48] J. Singh, A. Chauhan, Overview of wear performance of aluminium matrix composites reinforced with ceramic materials under the influence of controllable variables, Ceram. Int. 42 (1) (2016) 56–81, https://doi.org/10.1016/j.ceramint.2015.08.150.

[49] M. Walczak, D. Pieniak, M. Zwierzchowski, The tribological characteristics of SiC particle reinforced aluminium composites, Arch. Civ. Mech. Eng. 15 (2015) 116–123, https://doi.org/10.1016/j.acme.2014.05.003.

[50] Q. Chen, Y. Yu, G. Ma, X. Sun, L. Lu, Dry sliding wear behavior and mild–severe wear transition of the AA2195-T6 alloy under different loads, Crystals 13 (2023) 698, https://doi.org/10.3390/cryst13040698.

[51] R. Gupta, S. Sharma, T. Nanda, O.P. Pandey, Wear studies of hybrid AMCs reinforced with naturally occurring sillimanite and rutile ceramic particles for brake-rotor applications, Ceram. Int. 46 (10) (2020) 16849–16859, https://doi.org/10.1016/j.ceramint.2020.03.262.

[52] P.J. Blau, B.C. Jolly, J. Qu, W.H. Peter, C.A. Blue, Tribological investigation of titanium-based materials for brakes, Wear 263 (2007) 1202–1211, https://doi.org/10.1016/j.wear.2006.12.015.

[53] A. Daoud, M.T. Abou El-khair, Wear and friction behavior of sand cast brake rotor made of A359-20 vol% SiC particle composites sliding against automobile friction material, Tribol. Int. 43 (2010) 544–553, https://doi.org/10.1016/j.triboint.2009.09.003.

[54] S. Sharma, T. Nanda, O.P. Pandey, Effect of dual particle size (DPS) on dry sliding wear behaviour of LM30/sillimanite composites, Tribol. Int. 123 (2018) 142–154, https://doi.org/10.1016/j.triboint.2017.12.031.

[55] M.J. Ghazali, W.M. Rainforth, H. Jones, The wear of wrought aluminium alloys under dry sliding conditions, Tribol. Int. 40 (2007) 160–169, https://doi.org/10.1016/j.triboint.2005.09.009.

[56] M. Elmadagli, T. perry, A.T. Alpas, A parametric study of the relationship between microstructure and wear resistance of Al–Si alloy, Wear 262 (2007) 79–92, https://doi.org/10.1016/j.wear.2006.03.043.

[57] A.K. Prasada, K. Das, B.S. Murty, M. Chakraborty, Microstructure and the wear mechanism of grain-refined aluminum during dry sliding against steel disc, Wear 264 (7–8) (2008) 638–647, https://doi.org/10.1016/j.wear.2007.05.010.

[58] M.J. Ghazali, W.M. Rainfoth, M.Z. Omar, A comparative study of mechanically mixed layers (MMLs) characteristics of commercial aluminium alloys sliding against alumina and steel sliders, J. Mater. Process. Technol. 201 (2008) 662–668, https://doi.org/10.1016/j.jmatprotec.2007.11.158.

[59] J.M. Sanchez, H. Galarraga, E. Del Molino, J. Albizuri, T. Guraya, S.W. Hudson, Microstructure and mechanical properties of two novel scrap tolerant $Al_{65}Cu_{10}Mg_{10}Si_{10}Zn_5$ and $Al_{80}Cu_5Mg_5Si_5Zn_5$ high entropy aluminum alloys, Intermetallics 162 (2023) 1–13, https://doi.org/10.1016/j.intermet.2023.108023.

[60] F. Bonollo, N. Gramegna, G. Timelli, High-pressure die-casting: contradictions and challenges, J. Occup. Med. 67 (2015) 901–908, https://doi.org/10.1007/s11837-015-1333-8.

[61] S. Otarawanna, C.M. Gourlay, H.I. Laukli, A.K. Dahle, Formation of the surface layer in hypoeutectic Al-alloy high-pressure die castings, Mater. Chem. Phys. 130 (2011) 251–258, https://doi.org/10.1016/j.matchemphys.2011.06.035.

[62] S. Mezlini, Ph Kapsa, C. Henon, J. Guillemenet, Abrasion of aluminium alloy: effect of subsurface hardness and scratch interaction simulation, Wear 257 (2004) 892–900, https://doi.org/10.1016/j.wear.2004.05.004.

[63] T.M. Devenport, J.M. Griffin, B.F. Rolfe, M.P. Pereira, Friction and wear in stages of galling for sheet metal forming applications, Lubricants 11 (2023) 288, https://doi.org/10.3390/lubricants11070288.

[64] ASTM International, ASTM G99-05 - Standard Test Method for Wear Testing with a Pin-On-Disk Apparatus, ASTM International, West Conshohocken, 2010, pp. 1–5.

[65] G. Maculotti, E. Goti, G. Genta, L. Mazza, M. Galetto, Uncertainty-based comparison of conventional and surface topography-based methods for wear volume evaluation in pin-on-disc tribological test, Tribol. Int. 165 (2022) 1–18, https://doi.org/10.1016/j.triboint.2021.107260.

[66] A. Torres Pérez, A. Hernández Battez, G. García-Atance, J.L. Viesca, R. González, M. Hadfield, Use of optical profilometry in the ASTM D4172 standard, Wear 271 (11–12) (2011) 2963–2967, https://doi.org/10.1016/j.wear.2011.06.016.

[67] P. Pawlus, A. Dzierwa, Wear analysis of discs and balls on a micro-scale, Teh. Vjesn. 25 (2) (2018) 299–305, https://doi.org/10.17559/TV-20160530222544.

[68] J. Gobrecht, Settling-out of Fe, Mn and Cr in Al-Si casting alloys, Giessereiforschung 62 (1975) 263–266.

[69] J.L. Jorstad, Understanding sludge, Die Cast. Eng. 30 (1986) 30–36.

[70] L. Sun, Y.Y. Guo, L. Chen, G.Q. Zhao, Effects of solution and ageing treatments on the microstructure and mechanical properties of cold rolled 2024 Al alloy sheet, J. Mater. Res. Technol. 12 (2021) 1126–1142, https://doi.org/10.1016/j.jmrt.2021.03.051.

[71] Y.J. Kwon, I. Shigematsu, N. Saito, Mechanical property improvements in aluminum alloy through grain refinement using friction stir process, Mater. Trans. 45 (2004) 2304–2311.

[72] B.J. Jung, H.K. Lee, H.C. Park, Effect of grain size on the indentation hardness for polycrystalline materials by the modified strain gradient theory, Int. J. Solid Struct. 50 (2013) 2719–2724.

[73] Y. Liu, S. Ma, M.C. Gao, C. Zhang, T. Zhang, H. Yang, Z. Wang, J. Qiao, Tribological properties of AlCrCuFeNi2 high-entropy alloy in different conditions, Metall. Mater. Trans. A Phys. Metall. Mater. Sci. 47 (2016) 3312–3321, https://doi.org/10.1007/s11661-016-3396-8.

[74] W. Hong, W. Cai, S. Wang, M. Tomovic, Mechanical wear debris feature, detection, and diagnosis: a review, Chin. J. Aeronaut. 31 (5) (2018) 867–882, https://doi.org/10.1016/j.cja.2017.11.016.

[75] H.L. Costa, M.M. Oliveira Junior, J.D.B. de Mello, Effect of debris size on the reciprocating sliding wear of aluminium, Wear 376–377 (2017) 1399–1410, https://doi.org/10.1016/j.wear.2016.10.025.

[76] M.M. De Oliveira, H.L. Costa, W.M. Silva, J.D.B. De Mello, Effect of iron oxide debris on the reciprocating sliding wear of tool steels, Wear 426–427 (2019) 1065–1075, https://doi.org/10.1016/j.wear.2018.12.047.

[77] H.J. Kim, W. Windl, D. Rigney, Structure and chemical analysis of aluminum wear debris, Acta Mater. 55 (19) (2007) 6489–6498, https://doi.org/10.1016/j.actamat.2007.08.013.

[78] M.O.A. Mokhtar, The effect of hardness on the frictional behaviour of metals, Wear 78 (1982) 297–304, https://doi.org/10.1016/0043-1648(82)90240-X.

[79] S. Martin, S. Kandermir, M. Antonov, Investigation of the high temperature dry sliding wear behavior of graphene nanoplatelets reinforced aluminum matrix composites, J. Compos. Mater. 0 (2020) 1–14, https://doi.org/10.1177/0021998320979037.

[80] H. Zhu, C. Jar, J. Song, J. Zhao, J. Li, Z. Xie, High temperature dry sliding friction and wear behavior of aluminum matrix composites (Al3Zr+Al2O3)/Al, Tribology 48 (2012) 78–86, https://doi.org/10.1016/j.triboint.2011.11.011.

[81] C. Bellini, V. Cpccp, D. Lacoviello, F. Lacoviello, Temperature influence on brake pad friction coefficient modelisation, Materials 17 (2024) 189, https://doi.org/10.3390/ma17010189.

[82] N. Valizade, Z. Farhat, A review on abrasive wear of aluminum composites: mechanisms and influencing factors, J. Compos. Sci. 8 (2024) 149, https://doi.org/10.3390/jcs8040149.

[83] Classification of wear processes, Tribol. 10 (1987) 80–131, https://doi.org/10.1016/S0167-8922(08)70722-3.

[84] Y. Ozmen, Micromechanical approach to wear mechanisms, J. Eng. Sci. 2 (1995) 145–152.

[85] A. Fischer, W. Dudzinski, B. Gleising, P. Stemmer, Analyzing mild- and ultra-mild sliding wear of metallic materials by transmission electron microscopy, Adv. Anal. Methods Tribol. 2 (2018) 29–59.

[86] V.F. Sousa, F.J.G. Silva, Recent advances on coated milling tool technology—a comprehensive review, Coatings 10 (2020) 235, https://doi.org/10.3390/coatings10030235.

[87] K.H. Zum, Microstructure and wear of materials, Tribol. 10 (1987) 1–560.

[88] Z.B. Yusoff, S.B. Jamaludin, Tribology and development of wear theory: review and Discussion, in: Conf: Int. J. Curr. Res. Rev 3, 2011. India.

[89] M.A. Wimmer, M.P. Laurent, Tribology of the Artificial Hip, vol. 3, Fastest Musculoskeletal Insight Engine, 2016.

[90] N. Radhika, S. Ramanathan, S.V. Prasat, B. Anandavel, Dry sliding wear behaviour of aluminium/alumina/graphite hybrid metal matrix composites, Ind. Lubric. Tribol. 64 (2012) 259–366, doi.org/110.1108/00368791211262499.

[91] M.H. Abdelaziz, H.W. Doty, S. Valtierra, F.H. Samuel, Static versus dynamic thermal exposure of transition elements-containing Al-Si-Cu-Mg cast alloy, Mater. Sci. Eng., A 739 (2019) 499–512, https://doi.org/10.1016/j.msea.2018.09.096.

[92] L. Ceschini, A. Morri, S. Toschi, S. Johansson, S. Seifeddine, Effect of microstructure and overaging on the tensile behavior at room and elevated temperature of C355-T6 cast aluminum alloy, Mater. Des. 83 (2015) 626–634, https://doi.org/10.1016/j.matdes.2015.06.031.

[93] C. Cai, H.F. Geng, S.F. Wang, B.X. Gong, Z. Zhang, Microstructure evolution of AlSi10Mg (Cu) alloy related to isothermal exposure, Materials 11 (5) (2018) 809, https://doi.org/10.3390/ma11050809, 1-13.

[94] Bo Lin, Haoyu Li, Rui Xu, Yuliang Zhao, Huaqiang Xiao, Zhengqiang Tang, Shaobo Li, Thermal exposure of Al-Si-Cu-Mn-Fe alloys and its contribution to high temperature mechanical properties, J. Mater. Res. Technol. 9 (29) (2020) 1856–1865, https://doi.org/10.1016/j.jmrt.2019.12.018.

[95] S.H. Rhee, K.C. Ludema, Mechanisms of formation of polymeric transfer films, Wear 46 (1978) 231–240.

[96] G. Plasensia, A.T. Utigard, High temperature oxidation mechanism of dilute copper aluminium alloys, Corrosion Sci. 47 (2005) 1149–1163, https://doi.org/10.1016/j.corsci.2004.06.031.